HHS Public Access

Author manuscript

Cell Rep. Author manuscript; available in PMC 2023 October 23.

Published in final edited form as:

Cell Rep. 2023 February 28; 42(2): 112127. doi:10.1016/j.celrep.2023.112127.

Circadian regulator CLOCK promotes tumor angiogenesis in glioblastoma

Lizhi Pang[1,7], **Madeline Dunterman**[1,7], **Wenjing Xuan**[1], **Annette Gonzalez**[2], **Yiyun Lin**[3,4], **Wen-Hao Hsu**[4,5], **Fatima Khan**[1], **Robert S. Hagan**[6], **William A. Muller**[2], **Amy B. Heimberger**[1], **Peiwen Chen**[1,8,*]

[1]Department of Neurological Surgery, Feinberg School of Medicine, Northwestern University, Chicago, IL 60611, USA

[2]Department of Pathology, Northwestern University Feinberg School of Medicine, Chicago, IL 60611, USA

[3]Department of Genetics, The University of Texas MD Anderson Cancer Center, Houston, TX, USA

[4]UTHealth Graduate School of Biomedical Sciences, The University of Texas MD Anderson Cancer Center, Houston, TX, USA

[5]Department of Cancer Biology, The University of Texas MD Anderson Cancer Center, Houston, TX 77054, USA

[6]Division of Pulmonary Diseases and Critical Care Medicine, Department of Medicine, Marsico Lung Institute, University of North Carolina at Chapel Hill, Chapel Hill, NC, USA

[7]These authors contributed equally

[8]Lead contact

SUMMARY

Glioblastoma (GBM) is one of the most aggressive tumors in the adult central nervous system. We previously revealed that circadian regulation of glioma stem cells (GSCs) affects GBM hallmarks of immunosuppression and GSC maintenance in a paracrine and autocrine manner. Here, we expand the mechanism involved in angiogenesis, another critical GBM hallmark, as a potential basis underlying CLOCK's pro-tumor effect in GBM. Mechanistically, CLOCK-directed olfactomedin like 3 (OLFML3) expression results in hypoxia-inducible factor 1-alpha (HIF1α)-

*Correspondence: peiwen.chen@northwestern.edu.

AUTHOR CONTRIBUTIONS

L.P. and M.D. performed most experiments. W.X. performed several *in vitro* studies. A.G. and W.A.M. isolated and generated iHUVECs. Y.L. and W.-H.H. performed single-cell analysis. F.K. assisted some *in vitro* and *in vivo* studies. R.S.H., W.A.M., and A.B.H commented on the research and provided mouse models. P.C. conceived the project and wrote the manuscript. All authors participated in editing the paper.

DECLARATION OF INTERESTS

The authors declare no competing interests.

SUPPLEMENTAL INFORMATION

Supplemental information can be found online at https://doi.org/10.1016/j.celrep.2023.112127.

mediated transcriptional upregulation of periostin (POSTN). As a result, secreted POSTN promotes tumor angiogenesis via activation of the TANK-binding kinase 1 (TBK1) signaling in endothelial cells. In GBM mouse and patient-derived xenograft models, blockade of the CLOCK-directed POSTN-TBK1 axis inhibits tumor progression and angiogenesis. Thus, the CLOCK-POSTN-TBK1 circuit coordinates a key tumor-endothelial cell interaction and represents an actionable therapeutic target for GBM.

In brief

Pang et al. show that circadian regulator CLOCK promotes tumor angiogenesis in glioblastoma (GBM) through regulation of the OLFML3-HIF1α-POSTN-TBK1 circuit. Disrupting the tumor-endothelial cell interaction by depletion of POSTN and TBK1 inhibits angiogenesis and tumor growth in GBM mouse and PDX models.

Graphical Abstract

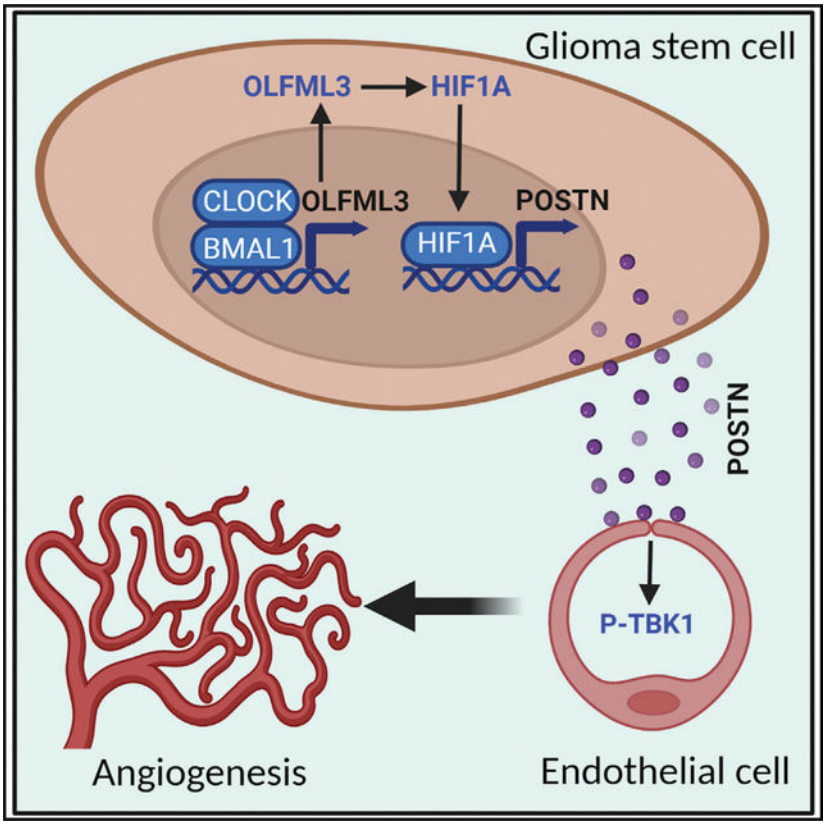

INTRODUCTION

Glioblastoma (GBM) is a devastating human malignancy, most commonly occurring in adults. The current standard of care only offers modest and transient relief for patients with GBM,[1–4] and the median survival is still approximately 20 months.[5] Moreover, efforts toward developing novel targeted therapies, such as those against receptor tyrosine kinase signaling, have failed in the clinic due to intratumoral heterogeneity.[1,2,6] Glioma stem

cells (GSCs) are a subpopulation of glioma cells that harbor stem cell-like properties and play an important role in regulating tumor initiation, evolution, and treatment resistance.[7,8] However, increasing evidence shows that the signaling of GSCs not only affects the cell intrinsic biological properties (e.g., stemness) but also regulates the biology of the tumor microenvironment (TME), including the most abundant macrophages and microglia.[1,2,8–10] One important mechanism by which GSCs interact with the TME is the circadian regulation by CLOCKs, which include transcriptional activators (e.g., the CLOCK-BMAL1 complex) and repressors (e.g., cryptochrome 1 and 2 [CRY1 and CRY2], period 1, 2, and 3 [PER1, PER2 and PER3], and REV-ERBα [also known as NR1D1]).[11] Our recent studies have shown that the CLOCK-BMAL1 complex in GSCs can upregulate the expression of chemokines, thus triggering the infiltration of immunosuppressive microglia into the GBM TME through a cell non-autonomous mechanism.[1,12] Together, these findings highlight a critical GSC-microglia interplay in GBM and provide a framework from which to identify therapeutic targets intercepting the GSC-TME crosstalk in GBM.

Angiogenesis is a prominent TME-associated hallmark of GBM.[13,14] Previous studies have shown that GSCs can promote tumor angiogenesis through distinct mechanisms, such as the secretion of pro-angiogenic factors and extracellular vesicles[15–17] and their differentiation into pericytes.[18] These findings gain added significance, as they suggest a critical connection between GSCs and endothelial cells/pericytes. However, the molecular basis underlying this connection remains enigmatic. A growing body of evidence demonstrates that the CLOCK-BMAL1 complex can affect both developmental and tumor angiogenesis. For example, disruption of the CLOCK-BMAL1 complex in a zebrafish embryonic model impairs vascular development and in cancer cells reduces tumor angiogenesis in colorectal cancer.[19,20] Thus, these findings highlight a crucial role of the CLOCK-BMAL1 complex in influencing angiogenesis in both physiological and pathological conditions. On the other hand, we and others have demonstrated that the CLOCK-BMAL1 complex is critical for maintaining GSC stemness in GBM.[1,21] Together, these findings led us to hypothesize that the CLOCK-BMAL1 complex might promote tumor progression by connecting GSCs and angiogenesis in GBM.

Here, we reveal a key function of GSC-derived CLOCK in promoting tumor angiogenesis in GBM. Mechanistically, the CLOCK-BMAL1 complex in GSCs modulates the olfactomedin like 3 (OLFML3)-hypoxia-inducible factor 1-alpha (HIF1α) axis to upregulate periostin (POSTN), which, in turn, promotes tumor angiogenesis via activation of the TANK-binding kinase 1 (TBK1) signaling in endothelial cells. *In vivo* studies with inhibition of POSTN and TBK1 in GBM mouse models, followed by clinical-pathological validations using GBM patient tumors, highlight the CLOCK-POSTN-TBK1 axis as a promising therapeutic target for GBM.

RESULTS

GSC-derived CLOCK promotes angiogenesis in GBM

To explore CLOCK regulation of GSC-TME interactions, gene set enrichment analysis (GSEA) was used to catalog hallmark pathways[22] in the TCGA GBM dataset with *BMAL1*-high versus *BMAL1*-low tumors.[23] Angiogenesis was one of the top hallmark pathways

enriched in *BMAL1*-high GBM patient tumors compared with *BMAL1*-low tumors (Figures 1A and 1B). Moreover, GSEA on Gene Ontology Biological Process (GOBP) signatures revealed that three angiogenesis-related signatures were enriched in *CLOCK*- and *BMAL1*-high GBM patient tumors compared with *CLOCK*- and *BMAL1*-low tumors, respectively (Figures S1A–S1F). To confirm the role of GSC-derived CLOCK in this process, we performed GSEA on microarray data from GBM patient-derived GSC272 cells with or without CLOCK depletion. The enrichment of angiogenesis signature was impaired in GSC272 cells expressing inducible short hairpin RNA (shRNA) CLOCK (ish*CLOCK*) compared with ish control (ishC) (Figure 1C). In order to obtain direct evidence, shRNA-mediated depletion of CLOCK and BMAL1 was performed in mouse QPP7 GSCs, a GSC line isolated from GBM tumors of an engineered mouse model with null alleles for *Qki*, *Pten*, and *Trp53*.[24] Transwell migration and tube formation assays demonstrated that the angiogenic potential of endothelial cells was dramatically reduced when they were treated with conditioned media (CMs) from GSCs that had the CLOCK-BMAL1 complex inhibited. Specifically, the migration and tube formation of primary mouse brain endothelial cells and immortalized human umbilical vein endothelial cells (iHUVECs) were inhibited by shRNA-mediated depletion of CLOCK (Figures 1D–1H and S1G) and BMAL1 (Figures 1I–1K and S1H–S1J) in QPP7 GSCs. Next, we used our ishRNA knockdown system[1] to deplete CLOCK in human GSC272 cells. Similarly, the migration and tube formation of iHUVECs were reduced by CMs from GSC272 cells expressing ish*CLOCK* compared with ishC (Figures 1L, 1M, S1K, and S1L). To rule out the potential effect of GSC-derived CLOCK in regulation of endothelial cell survival, we performed flow cytometry analyses and found that CMs from CLOCK-depleted GSC272 cells did not affect survival and apoptosis of iHUVECs (Figures S1M–S1P). Recently, we have demonstrated that genetic depletion of CLOCK in an orthotopic GSC272 model significantly extended survival.[1] To investigate whether the *in vivo* anti-tumor effects relate to tumor angiogenesis, we performed immunofluorescence staining for CD31 in ishC and ish*CLOCK* GSC272 tumors. The number of $CD31^+$ blood vessels in tumors was substantially reduced upon CLOCK depletion (Figures 1N and 1O). Endothelial cells can be differentiated from $CD34^+$ progenitor cells.[25] We further found that the migration of mouse and human primary $CD34^+$ cells was reduced when they were treated with CMs from GSC272 and QPP7 GSCs harboring CLOCK and BMAL1 depletion (Figures S2A–S2H). In summary, these data demonstrate that genetic depletion of the CLOCK-BMAL1 complex in GSCs impairs tumor angiogenesis *in vitro* and *in vivo*.

As an agonist of REV-ERB, SR9009 can inhibit the expression of CLOCK and BMAL1 in GSCs.[12] Accordingly, CMs from SR9009-treated GSC272 cells inhibited endothelial cell migration and tube formation *in vitro* (Figures 1P, 1Q, S2I, and S2J). Moreover, SR9009 treatment in C57BL/6 mice implanted with CT2A cells, a glioma cell line isolated from a carcinogen-induced tumor possessing a GSC-like phenotype,[12,26] significantly extended survival[1] and reduced the number of intratumoral $CD31^+$ blood vessels (Figures 1R and S2K). Clinically, the expression of a 20-gene angiogenesis signature[27] correlated positively with *CLOCK* and *ARNTL* (encoding for BMAL1) in TCGA GBM patient tumors (Figures S2L and S2M). Using this angiogenesis signature, unsupervised clustering was performed to categorize TCGA GBM into angiogenesis-high and angiogenesis-low

subgroups (Figure 1S). Angiogenesis-high tumors showed higher *CLOCK* and *ARNTL* expression compared with angiogenesis-low tumors (Figures 1T and 1U). Taken together, these findings demonstrate that GSC expression of the CLOCK-BMAL1 complex promotes tumor angiogenesis in GBM.

The CLOCK-BMAL1 complex promotes angiogenesis via upregulating POSTN in GSCs

To elucidate the factors governing CLOCK-dependent angiogenesis, enriched genes within the angiogenesis hallmark pathway were determined in TCGA GBM patient tumors (*BMAL1* high versus *BMAL1* low) and GSC272 cells (ishC versus ish*CLOCK*). Four angiogenesis-related genes (*PF4*, *ITGAV*, *LPL*, and *POSTN*) were identified to be regulated by the CLOCK-BMAL1 complex (Figure 2A). Among them, *POSTN* showed the most dramatic reduction upon CLOCK depletion in GSC272 cells (Figures 2B and 2C). qRT-PCR demonstrated that *POSTN* expression levels were dramatically reduced upon CLOCK depletion in GSC272 cells (Figure 2D) and upon SR9009 treatment in QPP7 GSCs (Figure 2E). Western blotting also confirmed that shRNA-mediated depletion of CLOCK (Figure 2F) and BMAL1 (Figure 2G) and SR9009 treatment (Figures 2H and 2I) significantly reduced the protein level of POSTN in QPP7 GSCs and GSC272 cells. To confirm the circadian regulation of POSTN, we monitored the mRNA levels of *CLOCK*, *ARNTL*, and *POSTN* in GSCs and found that they showed similar circadian oscillation in GSC272 and QPP7 GSCs (Figures S3A and S3B). Clinically, correlation analyses in TCGA and Chinese Glioma Genome Atlas (CGGA) GBM datasets demonstrated that *POSTN* expression in tumors correlated positively with *CLOCK* and *ARNTL* (Figures 2J, 2K, and S3C). Next, we performed analyses on single-cell RNA sequencing (scRNA-seq) data from a cohort of 28 GBM patient tumors.[28] Within the malignant population (Figure S3D), CD44 was used as a marker to classify GSCs (Figure S3E), and three discrete GSC subsets were identified (Figure S3F). *POSTN* was highly expressed in all three GSC subsets (Figure S3G). Based on the expression level of *ARNTL* (Figure S3H), we categorized GSCs into *ARNTL* negative (−) and positive (+) subgroups and found that *POSTN* expression level in the *ARNTL* (+) group was significantly higher than that in *ARNTL* (−) group (Figure 2L). Together, these findings indicate that *POSTN* is regulated by the CLOCK-BMAL1 complex in GSCs.

To validate whether GSC-derived POSTN functions as a pro-angiogenic factor in GBM, we performed angiogenic assays and showed that recombinant POSTN-supplemented media increased endothelial cell migration and tube formation (Figures S4A–S4D). Conversely, CMs from shRNA-mediated POSTN-depleted GSC272 (Figures 3A–3D and S4E), QPP7 GSCs (Figures 3E, 3F, and S4F–S4H), and CT2A cells (Figures S4F and S4I–S4L) showed impaired endothelial cell migration and tube formation compared with the CMs from shRNA controls. To confirm whether POSTN depletion affects tumor biology, we performed a series of cellular experiments and demonstrated that POSTN depletion did not affect the proliferation, apoptosis, and cell cycle of CT2A cells (Figures S5A–S5H). To confirm the importance of POSTN in tumor progression and angiogenesis *in vivo*, shC and sh*Postn* QPP7 and CT2A cells were implanted into the brains of C57BL/6 mice. The result demonstrated that POSTN depletion significantly extended the survival of tumor-bearing mice (Figures 3G, 3H, and S5I). Immunofluorescence for CD31 in shC and sh*Postn* tumors revealed that tumor angiogenesis was significantly reduced by POSTN depletion in QPP7

and CT2A models (Figures 3I, 3J, S5J, and S5K). Tumor-associated macrophages play an important role in angiogenesis.[2] We found that POSTN depletion reduced intratumoral F4/80$^+$CD206$^+$ macrophages in QPP7 and CT2A GBM models (Figures S5L–S5O), which is consistent with a previous report.[9] These findings collectively suggest that CLOCK-regulated POSTN is essential for tumor angiogenesis and GBM progression.

To reinforce the clinical relevance of our findings that CLOCK-regulated POSTN contributes to tumor angiogenesis, we performed analyses on scRNA-seq data from a cohort of 16 patients with GBM,[29] which contain both glioma cells and TME components, including immune cells, endothelial cells, and pericytes. Consistently, we confirmed that POSTN was highly expressed in CD44$^+$ GSCs (Figures 3K–3M). Based on the expression level of *POSTN*, patient tumors were categorized into two subgroups of *POSTN* high and *POSTN* low. GSEA on hallmark pathways in both glioma cells and endothelial cells demonstrated that angiogenesis was one of the top hallmark pathways enriched in *POSTN*-high patient tumors compared with *POSTN*-low patient tumors (Figures S6A and S6B). Moreover, *POSTN* expression level in GSCs was observed to be correlated positively with the abundance of endothelial cells, but not immune cells and pericytes, in GBM patient tumors (Figure 3N). Similarly, endothelial cell frequency was higher in *POSTN*-high tumors than that in *POSTN*-low tumors (Figure 3O). Finally, we performed *in silico* analyses on the TCGA GBM dataset. GSEA on GOBP signatures in TCGA GBM patient tumors showed that the expression of *POSTN* correlated positively with angiogenesis, blood vessel morphogenesis, and endothelial cell differentiation (Figure S6C). Unsupervised clustering with the angiogenesis signature[27] demonstrated that angiogenesis-high GBMs showed higher *POSTN* expression relative to angiogenesis-low tumors (Figure S6D). *POSTN* expression level correlated positively with the angiogenesis signature (Figure S6E)[27] and angiogenesis-associated marker genes, such as *PECAM1* (encoding for CD31; Figure S6F) and *CD34* (Figure S6G). Finally, the survival analysis demonstrated that the expression of *POSTN* was found to negatively correlate with patient overall survival in the TCGA GBM/low-grade glioma (LGG) dataset (Figure S6H) and the TCGA GBM dataset (Figure S6I).

CLOCK-directed OLFML3-HIF1α axis upregulates POSTN expression and angiogenesis

To investigate whether the CLOCK-BMAL1 complex can transcriptionally regulate *POSTN* in GSCs, the BMAL1 chromatin immunoprecipitation (ChIP)-seq dataset[21] from human neural stem cells (NSCs; e.g., hNP1 and ENSA) and GSCs (e.g., T3565 and T387) was analyzed. We did not observe binding of *BMAL1* to the *POSTN* promoter in either NSCs or GSCs (Figure S7A), suggesting that the CLOCK-BMAL1 complex may upregulate POSTN via an indirect regulation mechanism. Given that our recent studies have demonstrated that the CLOCK-BMAL1 complex promotes microglial infiltration via transcriptionally upregulating *OLFML3* and *HIF1A*,[1,12] we hypothesized a connection between the OLFML3-HIF1α axis and POSTN in GSCs. Bioinformatics analyses demonstrated that *POSTN* was the top gene enriched in *OLFML3*-high GBM patient tumors (Figure 4A) and correlated positively with *OLFML3* in TCGA GBM patient tumors (Figure 4B). Western blotting demonstrated that shRNA-mediated depletion of OLFML3 in GSC272 cells significantly reduced POSTN expression (Figure 4C). We have recently demonstrated that depletion of OLFML3 extended the survival of SCID mice bearing GSC272 tumors.[1]

To confirm whether OLFML3-depletion-induced tumor growth impairment relates to angiogenesis, we first performed a Transwell migration assay using the CMs from control and OLFML3-depleted GSC272 cells and found that *OLFML3* depletion dramatically reduced endothelial cell migration (Figures 4D and S7B). Next, immunohistochemistry staining for POSTN and CD31 was performed in shC and sh*OLFML3* GSC272 tumors, which demonstrated that POSTN expression and $CD31^+$ blood vessels were significantly reduced upon OLFML3 depletion (Figures 4E–4G). Together, these findings indicate that the pro-angiogenic factor POSTN is regulated by OLFML3 in GSCs.

Since HIF1α is a downstream signaling of OLFML3,[12] we further investigated whether POSTN is regulated by HIF1α in GSCs. Bioinformatics analyses demonstrated that *POSTN* was the top gene enriched in *HIF1A*-high tumors compared with *HIF1A*-low tumors (Figure S7C) and correlated positively with *HIF1A* in TCGA GBM patient tumors (Figure S7D). To confirm whether HIF1α can directly regulate POSTN, the JASPAR database was utilized, which revealed that putative HIF1A-binding elements were identified in the *POSTN* promoter and were evolutionarily conserved across different species, including human and mouse (Figures S7E and S7F). ChIP-PCR assay confirmed that HIF1A bound to the *POSTN* promoter in GSC272 cells (Figures 4H and 4I). qRT-PCR and western blotting assays demonstrated that inhibition of HIF1α using its inhibitor acriflavine (ACF) dramatically reduced the mRNA and protein levels of POSTN in GSC272 cells (Figures 4J and 4K). Functional studies showed that the migration and tube formation potential of endothelial cells was enhanced by GSC272 CM treatment, which was abolished when GSC272 cells were pretreated with ACF (Figures 4L, 4M, S7G, and S7H). Together, these findings indicate that the OLFML3-HIF1α axis is required for CLOCK-regulated POSTN expression and angiogenesis in GBM.

TBK1 mediates POSTN-induced tumor angiogenesis in GBM

To explore the potential molecular mechanisms underlying POSTN-directed angiogenesis, an unbiased GSEA in GBM patient tumors from the TCGA dataset was performed with *POSTN* high versus *POSTN* low and in endothelial cells from scRNA-seq GBM dataset[28] with *POSTN* high versus *POSTN* low in glioma cells/GSCs. By overlapping these two datasets, we identified three signature pathways (e.g., ESC_V6.5_UP_EARLY.V1_DN, ESC_V6.5_UP_LATE.V1_DN, and TBK1 signature) that were potentially regulated by POSTN (Figures 5A, S8A, and S8B). Among these three signature pathways, TBK1 is a druggable kinase, and the other two signatures are involved in early and late stages of differentiation of embryonic stem cells. Therefore, we decided to investigate whether TBK1 is required for POSTN-induced angiogenesis. To solidify the connection between angiogenesis and TBK1, expression patterns of angiogenic marker CD31 and phospho-TBK1 (P-TBK1; Ser172) were analyzed in mouse and human GBM tumor samples. Immunofluorescence staining demonstrated that P-TBK1 was highly expressed in $CD31^+$ blood vessels in GBM tumors from murine animal models (including CT2A and QPP7 GSC) and patients with GBM (Figure 5B). In our endothelial cell system, western blotting demonstrated that CT2A CMs upregulated P-TBK1, an effect that was abolished when CT2A cells express sh*Postn* (Figure 5C). To further confirm the role of POSTN in regulation of TBK1, endothelial cells were treated with POSTN recombinant protein that upregulated

TBK1 mRNA levels (Figure S8C) and induced TBK1 activation (as indicated by P-TBK1 level) in a time- and dose-dependent manner (Figures 5D and 5E). In tumors from QPP7 and CT2A GBM mouse models, shRNA-mediated POSTN depletion reduced P-TBK1-expressing blood vessels (Figure S8D–S8G). Thus, the POSTN-induced TBK1 activation is observed in endothelial cells of mouse and human GBM, prompting exploration of a potential role of TBK1 in mediating POSTN-induced angiogenesis in GBM.

Next, angiogenic assays showed that POSTN-induced endothelial cell migration and tube formation were abolished by TBK1 inhibition using its specific inhibitors, including BX-795 hydrochloride (BX795)[30,31] and compound 1 (CMPD1)[32] (Figures 5F, 5G, S8H, and S8I). A Matrigel plug assay also demonstrated POSTN-induced angiogenesis ($CD31^+$ cells) was impaired by the treatment with TBK1 inhibitors BX795 and CMPD1 (Figures S8J and S8K). Together, these findings support a role for TBK1 signaling in mediating POSTN-induced angiogenesis. To investigate the role of endothelial cell TBK1 in angiogenesis and tumor growth *in vivo*, we generated endothelial cell-specific TBK1 null (TBK1-eKO [knockout]) mice by crossing TBK1-flox mice with Cdh5(PAC)-CreERT2 mice (Figure 5H).[33] Orthotopic transplantation of QPP7 and CT2A cells into the brains of TBK1-eKO mice showed a survival extension compared with TBK1 wild-type (WT) mice (Figures 5I and 5J). Immunofluorescence staining confirmed that TBK1 in endothelial cells (Figure S8L) and $CD31^+$ blood vessels (Figures 5K and 5L) were dramatically reduced in tumors from TBK1-eKO mice compared with TBK1-WT mice. Moreover, treatment with TBK1 inhibitor BX795 in the GSC272 model resulted in reduction of intratumoral P-TBK1 signaling and blood vessels (Figures S8M–S8P). Finally, the clinical relevance of the above experimental findings was supported by the positive correlations among POSTN, P-TBK1, and CD31 in GBM patient tumors (Figures 5M–5P). Together, these findings highlight the importance of endothelial cell TBK1 in angiogenesis and glioma tumor biology.

DISCUSSION

In the current study, we revealed the CLOCK-BMAL1 complex as a key molecular switch controlling the connection between GSCs and endothelial cells in GBM. We identified POSTN as a critical pro-angiogenic factor that is regulated by the CLOCK-OLFML3-HIF1α axis in GSCs and promotes tumor angiogenesis via activation of the TBK1 signaling in endothelial cells. As a result, inhibition of POSTN in GSCs and TBK1 in endothelial cells impairs GBM tumor growth and angiogenesis. Clinically, we found that the expression of the CLOCK-POSTN-TBK1 axis correlates positively with tumor angiogenesis and negatively with overall survival in patients with GBM. Together, our study reveals the CLOCK-OLFML3-HIF1α-POSTN axis (in GSCs) and the POSTN-TBK1 axis (in endothelial cells) as key regulators mediating GSC-endothelial cell communication and as actionable therapeutic targets for GBM.

Circadian rhythm regulators (e.g., the CLOCK-BMAL1 complex) play an important role in tumorigenesis across cancer types.[34,35] Emerging evidence reveals that depletion of the CLOCK-BMAL1 complex in cancer cells has shown to inhibit leukemia stem cell proliferation, promote myeloid differentiation in acute myeloid leukemia,[36] and impair cancer cell proliferation and migration in GBM.[37] Moreover, we and others have shown that

the CLOCK-BMAL1 complex is essential for GSC stemness maintenance via regulating cell metabolism.[1,21] In addition to this cell-intrinsic effect, recent findings support the hypothesis of cell-extrinsic effects of the CLOCK-BMAL1 complex in regulating the TME.[11] In GBM, we have demonstrated that GSC-derived CLOCK functions as a suppressor of anti-tumor immunity via promoting the infiltration of immunosuppressive microglia.[1,12] In this study, we extend the actions of GSC-derived CLOCK as a promoter of tumor angiogenesis in GBM, consistent with recent reports showing that cancer cell-derived CLOCK promotes tumor angiogenesis in colorectal cancer.[19] Functionally, our work demonstrates that inhibition of the CLOCK-BMAL1 complex impairs tumor angiogenesis in GBM mouse models. In sum, our work reinforces the importance of the GSC-directed CLOCK-BMAL1 complex in regulating tumor angiogenesis and highlights a critical angiogenesis-related therapeutic potential via blockade of the CLOCK-BMAL1 complex in GBM.

Angiogenesis is a prominent cancer hallmark in solid tumors, including GBM.[13,14] Although good clinical responses have been obtained in some types of cancer, such as colorectal cancer, the anti-angiogenic therapy (e.g., anti-VEGF therapy) induces adverse effects since it can drive vascular alterations in healthy tissues.[38–40] In GBM, clinical trials have shown that anti-angiogenic therapy does not improve the overall survival of patients.[41] The basis for this therapeutic failure is unclear, but it is worth noting that angiogenesis regulation in GBM is context dependent. For example, *P14ARF* deficiency in GBM cells inhibits angiogenesis via upregulation of metalloproteinase-3,[42] whereas the rearrangement and activation of *EGFRvIII* promotes angiogenesis via the nuclear factor κB (NF-κB)-interleukin-8 pathway.[43] Consistent with previous studies,[9] our scRNA-seq analysis on GBM patient tumors suggests that POSTN is preferentially expressed by GSCs. In this study, we established that CLOCK-dependent POSTN supports tumor angiogenesis and GBM progression and is associated with poor clinical outcomes. Therefore, our study reinforces the importance of the CLOCK-BMAL1 complex in regulation of tumor angiogenesis and identifies POSTN as a potential target along with a specific CLOCK/BMAL1-high responder population for such intervention. In addition to directly promoting angiogenesis, as supported by our data in this study and other reports,[44] POSTN limits the tumor response to anti-angiogenic therapy in various cancer types, including GBM.[45,46] Together, these findings highlight the importance of the CLOCK-BMAL1 complex in regulating tumor angiogenesis and suggest that combined inhibition of POSTN and anti-angiogenic therapy may yield clinical benefits for CLOCK/BMAL1-high GBM.

POSTN, a multifunctional matricellular protein (also called osteoblast-specific factor), was first identified in osteoblasts, which displays an important role in regulating inflammatory responses and the TME.[47] It has been shown that POSTN is essential for macrophage and epithelial cell migration into the TME via binding to its receptors αVβ3 and αVβ5 integrins.[9,48] Along similar lines, it would be helpful to determine whether these integrins are required for CLOCK-directed POSTN signaling in GBM angiogenesis, thus expanding therapeutic targets for this intractable disease. Intriguingly, our unbiased pathway analysis, followed by functional studies, demonstrated that TBK1 is the key downstream signaling responsible for POSTN-induced angiogenesis in GBM. TBK1 is essential for type I interferon production during anti-viral immune responses.[49–51] TBK1 in cancer cells functions as an oncogene to regulate cell division, autophagy, and AKT pro-survival

signaling in melanoma and lung cancer,[52–54] and in GSCs, it serves to suppress the core pluripotency circuitry in GBM.[55] The function of TBK1 in angiogenesis is supported by a study showing that cancer cell TBK1 promotes tumor angiogenesis in a non-cell-autonomous mechanism via upregulating VEGF.[56,57] However, our work further reinforces the critical role of endothelial cell TBK1 in regulating POSTN-induced tumor angiogenesis in GBM. This identification, coupled with the anti-tumor effect of endothelial cell TBK1 deletion in GBM mouse models, provides guidance for clinical investigation of blocking angiogenesis as a strategy. Together, this study contributes to our understanding of TBK1, specifically in endothelial cells, in supporting tumor angiogenesis in GBM.

Limitations of the study

First, we observed an angiogenesis promoting effect of the CLOCK-BMAL1 complex via upregulating pro-angiogenic factor POSTN in GSCs and have shown that CLOCK is essential for GSC stemness maintenance.[1] However, in this article, we have not shown the direct evidence supporting the CLOCK-regulated connection between GSC stemness and angiogenesis in GBM. Second, we showed that GSC-derived POSTN promotes angiogenesis via activation of the TBK1 signaling. However, the detailed molecular mechanism for how POSTN activates TBK1, and subsequently promotes angiogenesis, is not understood well and is a future direction to pursue.

STAR★METHODS

RESOURCE AVAILABILITY

Lead contact—Further information and requests for resources and reagents should be directed to and will be fulfilled by the Lead Contact, Peiwen Chen (peiwen.chen@northwestern.edu).

Materials availability—This study did not generate new unique reagents.

Data and code availability—This paper analyses publicly available data. The references for these datasets are listed within the relevant results sections. This study does not report original code.

Any additional information required to reanalyze the data reported in this paper is available from the lead contact upon request.

EXPERIMENTAL MODEL AND SUBJECT DETAILS

Mice and intracranial xenograft tumor model—Female C57BL/6 (Jackson Laboratory, #0000664), SCID (Taconic Biosciences, #ICRSC-F) and nude (Jackson Laboratory, #007850) mice at 3–4 weeks of age were grouped by 5 animals and maintained under pathogen-free conditions. C57BL/6 TBK1-flox mice were a kind gift from Dr. Katherine Fitzgerald (University of Massachusetts) and have been described previously.[49] TBK1-flox mice were crossed with Cdh5(PAC)-CreERT2 mice (developed by Dr. Ralf Adams and provided by Dr. William A. Muller) to obtain TBK1-eKO mice. All animal experiments were performed with the approval of the Institutional Animal Care and Use

Committee (IACUC). The intracranial xenograft tumor models in C57BL/6 and SCID mice were established.[2] In brief, mice were anesthetized by intraperitoneal injection of a stock solution containing ketamine (Covetrus, #056344, 100 mg/kg) and xylazine (Akorn, #59399-110-20, 20 mg/kg) and were placed into the stereotactic apparatus (RWD Life Science, # 68513). A small hole was bored in the skull 1.2 mm anterior and 3.0 mm lateral to the bregma using a dental drill. Cells were injected in a total volume of 5 μL into the right caudate nucleus 3 mm below the surface of the brain using a 10 μL Hamilton syringe with an unbeveled 30-gauge needle. The incision was closed using Vetbond glue. Mice with neurologic deficits or moribund appearance were sacrificed. Following the transcardial perfusion with 4% PFA (Alfa Aesar, #J61899), brains were removed and fixed in formalin (Fisher Chemical, #SF100-4), and were processed for optimal cutting temperature (OCT)- and paraffin-embedded blocks.

GBM patient samples—Patient tumor samples (n = 23) from surgically-resected IDH-WT GBMs were collected at the Northwestern Central Nervous System Tissue Bank (NSTB). All patients were diagnosed according to the WHO diagnostic criteria by neuropathologist at the NSTB. Patient information is provided in Table S1. According to The George Washington University Institutional Review Board and based on the guidelines from the Office of Human Research Protection, the conducted research meets the criteria for exemption #4 (45 CFR 46.101(b) Categories of Exempt Human Subjects Research) and does not constitute human research.

METHOD DETAILS

Cell culture—293T and CT2A cells were cultured in Dulbecco's Modified Eagle's Medium (DMEM; Gibco, #11995-065) containing 10% fetal bovine serum (FBS; Fisher Scientific, #16140071) and 1:100 antibiotic-antimycotic (Gibco, #15140-122), and were purchased from the American Type Culture Collection (ATCC). For stemness maintenance, CT2A cells were cultured in neural stem cell (NSC) proliferation media (Millipore, #SCM005) containing 20 ng/mL basic fibroblast growth factor (bFGF; PeproTech, #100-18B) and epidermal growth factor (EGF; PeproTech, #AF-100-15). iHUVECs were made by transduction of HUVEC with LSNX-16E6E7, an amphotrophic retrovirus encoding the oncoproteins E6 and E7 of human papillomavirus type 16 (provided by Dr. David Klumpp; Northwestern University, Evanston, IL). iHUVECs display all the known characteristics of primary endothelial cells.[58,59] Human primary $CD34^+$ cells (#70002.1) were purchased from STEMCELL Technologies. iHUVECs and $CD34^+$ cells were cultured in endothelial cell basal medium (Gibco, #11111044) containing 12.5 mg/mL endothelial cell growth supplement (Corning, #356006), 10% FBS and 1:100 antibiotic-antimycotic. Patient-derived GSC272 and mouse QPP7 GSCs were cultured in NSC proliferation media (Millipore Corporation, Billerica, MA) containing 20 ng/mL bFGF and EGF. All cells were maintained at 37°C and 5% CO_2 and were confirmed to be mycoplasma-free.

Isolation and culture of primary mouse brain endothelial cells and $CD34^+$ hematopoietic stem and progenitor cells—Mouse brains were dissected and placed in a Petri dish containing cold phosphate-buffered saline (PBS; Fisher Scientific, #BP399500). Olfactory lobes, cerebellum, medulla, spinal cord, and meningeal layers were

removed. Each brain was individually minced into tiny pieces and transferred into a 50 mL conical tube with 1 mL of wash buffer containing IMDM (Cytiva, #SH30228.FS) and 2% FBS. 10 mL of a digestion mixture containing IMDM supplemented with 100 μg/mL collagenase I (usp, #1148089), 100 μg/mL collagenase II (MP Biomedicals, #0210050201), and 20 units/mL deoxyribonuclease I (Worthington, #LS002139) was added to each tube, and samples were incubated in a 37°C shaking incubator for 60–90 min. Following digestion, tissue samples were filtered through a 70 μM strainer (BioX, #15-1070-1) and centrifuged at 700 g for 5 min at 4°C. To each tube, 3 mL of ACK lysing buffer (Gibco, #A1049201) was added to incubate for 5–10 min at room temperature. After adding 5 mL PBS, samples were centrifuged 700 g for 5 min at 4°C. Then, magnetic-activated cell sorting (MACS) method was used to separate primary $CD31^+$ endothelial cells from $CD45^+$ immune cells in the brain. To this end, we first completed a CD45 positive selection using CD45 MicroBeads (Miltenyi Biotec, #130-052-301), and then the $CD45^-$ fraction samples were centrifuged at 300 g for 10 min. Cells were then incubated with CD31 MicroBeads (Miltenyi Biotec, #130-097-418). $CD45^-CD31^+$ endothelial cells were cultured in human endothelial media (Gibco, #11111044) supplemented with 10% FBS, 1% penicillin-streptomycin, and 12.5 mg/mL endothelial cell growth supplement, and maintained at 37°C with 5% CO_2. $CD34^+$ hematopoietic stem and progenitor cells were isolated from mouse bone marrow using EasySep Mouse Hematopoietic Progenitor Cell Isolation Kit (STEMCELL Technologies, #19856). Breifly, bone marrow cells were flushed from the femur and tibia using a 23 gauge needle. After centrifuge, cells were resuspended in RPMI 1640 media (Gibco, #22400-089) containing 10% FBS, 50 μM 2-mercaptoethanol (Sigma, #M7522), and 1:100 antibiotic-antimycotic at 1×10^8 cells/mL. Rat serum was used to block the unspecific bindings between samples and biotinylated antibodies. Samples were then loaded into a 5 mL polystyrene round-bottom tube and incubated with isolation cocktail and rapidSpheres sequentially. Negative isolation was performed using EasySep (Catalog #18000) magnet. This method allowed us to remove Lin^+ (CD3, CD11b, CD19, CD45R (B220), Ly6G/C (Gr-1), and TER119) mature erythroid, myeloid, and megakaryoid cells. The remaining hematopoietic stem and progenitor cells ($Lin^-SCA1^{-/low}c\text{-}Kit^+$, $CD34^+$, Thy^+) were pelleted and cultured in RPMI 1640 media containing 10% FBS.

Plasmids, viral transfections, and cloning—shRNAs targeting human *CLOCK, OLFML3* and *POSTN,* and mouse *Clock, Bmal1* and *Postn* in the pLKO.1 vector (Sigma, #SHC001) were used in the current study. Lentiviral particles (8 μg) were generated by transfecting 293T cells with the packaging vectors psPAX2 (4 μg; Addgene, #12260) and pMD2.G (2 μg; Addgene, #12259). Lentiviral particles were collected at 48 and 72 h after the transfection in 293T cells and filtered through a 0.45-μm filter. Receiving cells were infected with viral supernatant containing 10 μg/mL polybrene (Millipore, #TR-1003-G). After 48 h, cells were selected by puromycin (2 μg/mL; Millipore, #540411) and tested for the expression of CLOCK, BMAL1, OLFML3 and POSTN by immunoblots. The following mouse (*Clock*: #74: TRCN0000095686 and #86: TRCN0000306474; *Bmal1*: #54: TRCN0000095054 and #57: TRCN0000095057; POSTN: #9: TRCN0000111166 and #12: TRCN0000111169) and human (*CLOCK*: TRCN0000306475; *OLFML3*: #1: TRCN0000186745 and #3: TRCN0000203502; and *POSTN*: #2: TRCN0000123055 and #4: TRCN0000123057) shRNA sequences were selected for further use following the

validation. Doxycycline-inducible plasmids were generated by cloning the desired human shRNA sequences (*CLOCK*: TRCN0000306475) into a pLKO.1 vector through the Gateway Cloning System (Thermo Fisher Scientific, #12535029).

Angiogenesis assays—For the transwell migration assay, endothelial cells were suspended in serum-free culture medium treated with POSTN (R&D, # 3548-F2-050) recombinant protein in the presence and absence of TBK1 inhibitors BX795 (Selleck Chemicals, #S1274) and CMPD1 (Selleck Chem, #S8922) and seeded into 24-well transwell inserts (8.0 μm). In the other sets of transwell migration assays, conditioned media from GSCs or CT2A cells with or without CLOCK, BMAL1, POSTN and OLFML3 shRNAs, as well as SR9009 (Selleck Chemicals, #S8692) and ACF (Sigma, #A8126) treatment were added to the remaining receiver wells. After 24 h, the migrated endothelial cells were fixed and stained with crystal violet (0.05%, Sigma). Tube formation assay was carried out as described previously.[60] Briefly, 96-well plates or 24-well plates were coated with growth factor reduced matrigel (Corning, #354230). iHUVECs were treated with indicated CM, POSTN recombinant protein in the presence or absence of TBK1 inhibitors BX795 and CMPD1, and then seeded on this matrix, forming tubules within 24 h of plating. Transwell inserts or wells were visualized, and endothelial cell migration and tube formation were assessed using ImageJ (NIH). For the matrigel plug assay, growth factor-reduced matrigel supplemented with POSTN recombinant protein in the presence or absence of TBK1 inhibitor were subcutaneously injected into WT C57BL/6 mice. The plugs were removed for investigation of blood vessel density 7 days after implantation.

Immunoblotting—Immunoblotting was performed following a standard protocol. In brief, indicated cells were lysed on ice with RIPA buffer (Thermo Fisher Scientific, #89901) supplemented with protease inhibitor cocktail (Millipore, #11697498001). Samples were applied to SDS-PAGE gels (GenScript, #M00652) and blotted onto a nitrocellulose membrane (Bio-Rad, #1704270). Membranes were then incubated with primary antibodies (1:1,000 dilution) overnight at 4°C, and then incubated with HRP-conjugated secondary antibodies (1:1,000 dilution; Cell Signaling Technology (CST), #7076S and #7074S) for 1 h at room temperature. Signaling was exposed with chemiluminescence (Pierce, #34580 and #34076) using the ChemiDoc MP Imaging System (Bio-Rad, #17001402). Antibodies were purchased from the indicated companies, including b-actin (Sigma, #A3854), Vinculin (EMD Millipore, #05-386), CLOCK (CST, #5157S), BMAL1 (CST, #14020S), OLFML3 (Fisher, #PA5-31581), POSTN (Novus, #NBP1-30042), TBK1 (CST, #3504), and P-TBK1 (CST, #5483S).

Quantitative real-time PCR (RT-qPCR)—Cells were detached with trypsin (Gibco, #25300-054) or Accutase (Millipore, #SCR005) and then pelleted. RNA was isolated using the RNeasy Mini Kit (Qiagen, #74106), and then reverse-transcribed into cDNA with the All-In-One 5X RT MasterMix (Applied Biological Materials, #G592). PCR was performed using the SYBR Green PCR Master Mix (Bio-Rad, #1725275). Approximately 10 ng of template was used per PCR reaction. The expression of each gene was quantified using the ΔΔCt method and normalized to the housekeeping gene (e.g., *ACTB* or *GAPDH*). PCR was

run using the CFX Connect Real-Time PCR Detection System (Bio-Rad, #1855201). The primers used for RT-qPCR are listed in Table S2.

Immunofluorescence and immunohistochemistry—Immunofluorescence and immunohistochemistry were performed using a standard protocol. Briefly, a pressure cooker (Bio SB, #7008) was used for antigen retrieval using antigen unmasking solution (Vector Laboratories, #H-3301) at 95°C for 30 min. After blocking with 10% goat serum for 1 h, slides were incubated with primary antibodies (1:200) overnight at 4°C. Slides were then washed with PBS and incubated with secondary antibodies (Life Technologies, 1:500) for 1 h at room temperature. For immunofluorescence, slides were counterstained with DAPI/anti-fade mounting medium (Vector Laboratories, #H-1200-10). Signal of protein was captured by using Nikon AX/AX R Confocal Microscope System in the Center for Advanced Microscopy (CAM) at Northwestern University. The staining signaling was analyzed using ImageJ (NIH, Bethesda, ML). For immunohistochemistry, the staining was developed with DAB Quanto (Epredia, #TA125QHDX). The nuclear was stained with hematoxylin and then images were captured using EVOS Cell Imaging System. ImageJ with IHC profiler plug-in was used to score positive signals.[61] Antibodies specific to CD31 (Novus Biologicals, #NBP2-80640), P-TBK1 (CST, #5483S), CD206 (R&D, #AF2535), F4/80 (CST, #70076S) and POSTN (Novus, #NBP1-30042) were used.

Chromatin immunoprecipitation sequencing and ChIP-PCR—GSE134974 containing BMAL1 chromatin immunoprecipitation sequencing (ChIP-seq) data[21] in patient-derived GSCs and normal human NSCs was enrolled in this study and the data were analyzed by the Integrative Genomics Viewer (Broad Institute). ChIP-PCR was performed using the commercial Pierce™ Magnetic CHIP kit (ThermoFisher, #26157) according to the manufacturer's instruction. Briefly, GSC272 cells were cross-linked with 1% PFA for 10 min, and then reactions were quenched with the use of glycine for 5 min at room temperature. Cells were incubated with Membrane Extraction Buffer for 10 min on ice, then lysed using MNase Digestion Buffer at 37°C for 15 min, after which a stop solution was added to halt the reaction. Chromatin fragmentation was performed using sonication, and solubilized chromatin was then incubated with HIF1α antibodies (CST, #3716S) overnight at 4°C. IP reactions were mixed with ChIP Grade Protein A/G Magnetic Beads for 2 h at 4°C. After collecting the beads with a magnetic stand separator and washing, elution and reverse-crosslinking were performed in elution buffer containing proteinase K (20 mg/mL) and NaCl (5 M) at 65°C for 1.5 h. Eluted DNA was purified using the provided purification kit and then used to perform qPCR. PCR products were also visualized via gel electrophoresis on a 2% agarose gel. The POSTN primers (as shown in Table S2) were designed according to the E-box of human *POSTN* gene.

Apoptosis analysis—The apoptosis of CT2A cells with or without POSTN knockdown was evaluated using Apotracker Green (BioLegend, #427402).[62] Briefly, 10^5 cells were stained with Apotracker (1:10 dilution) and then 5 μL propidium iodide (PI) solution (BioLegend, # 421301) was added to label late apoptotic and necrotic cells. After washing with PBS, FITC and PI signals were analyzed in BD FACSymphony flow cytometer.

Proliferation analysis—The proliferation of control and sh*Postn* CT2A cells was assayed through colony formation. Briefly, cells (5×10^3) were seeded in each well of 6-well plates and cultured for 5–7 days. At the endpoint, cells were fixed and stained with 0.5% crystal violet in 25% methanol for 1 h. On the other hand, the proliferation of CT2A cells was investigated using CellTrace CFSE Cell Proliferation Kit (Invitrogen, #C34554). To this end, 10^6 cells were harvested and incubated with CFSE working solution (1:1000) for 20 min at 37°C. After the incubation, the staining was stopped by adding complete cell culture medium. Cells were collected for flow cytometry analysis after 5 days of culture in the dark. The number of CFSE-positive peaks was analyzed using ImageJ.

Cell cycle analysis—Control and sh*Postn* CT2A cells were harvested and incubated with 70% ethanol for 30 min on ice. After washing with PBS, cells were treated with 100 μL ribonuclease (100 μg/mL) for 5 min at room temperature to remove RNA fragments. 400 μL PI (50 μg/mL) was then added to stain the DNA content. Data was acquired in BD FACSymphony flow cytometer. The measurement of cell cycle parameters was analyzed using FlowJo.

Microarray analysis—Microarray data of GEO, GSE140409, containing gene expression data of ishC and ish*CLOCK* GSC272 cells,[1] was enrolled in this study. The gene expression in human GBM was analyzed using gene-profiling data from the TCGA datasets.

GSEA analysis—GSEA was performed using the GSEA software 4.1.0 from the Broad Institute (http://www.broad.mit.edu/gsea/software/software_index.html). The gene expression data were microarray data from public available GEO and TCGA datasets. The hallmark and gene Ontology Biological Process (GOBP) signatures were downloaded from the Molecular Signatures Database (http://software.broadinstitute.org/gsea/msigdb/index.jsp). The normalized enrichment score (NES) and false discovery rate (FDR) were acquired by the analysis. A gene set is considered significantly enriched when an FDR is < 0.25.

Single-cell sequencing data analysis—Single-cell sequencing data of GEO, GSE131928,[28] were used to perform unsupervised sub-clustering for GSCs. GSC clustering was performed within the malignant population, and CD44 was selected as the positive control. GSC sub-clustering was performed using principal component analysis with the number of principal components from the elbow point of scree plot. For the differential gene expression of *ARNTL* within the GSC subcluster, cells were divided into $ARNTL^+$ and $ARNTL^-$ subgroups. The expression of *ARNTL* and *POSTN* in the total GSC population and subgroups were analyzed. Next, the single-cell sequencing data of GEO, GSE182109,[29] was used to analyze the connection among glioma cells/GSCs, POSTN, immune cells, and angiogenesis in GBM patient tumors. Canonical markers and cluster differential genes were used to identify distinct cell types in GBM tumors. For the differential gene expression of *POSTN* within the glioma cell subcluster, cells were divided into two groups: *POSTN*-high and *POSTN*-low subgroups. DESeq2 v 1.30.0 was performed to obtain the rank list of the differential genes in glioma cells and/or endothelial cells for GSEA. Differential gene analysis was based on the non-parametric Wilcoxon rank-sum test. Genes with adjusted

p value < 0.05 were further used for gene set enrichment analysis by fgsea R package. Resolutions from 0.1 to 1 were explored for reasonable sub-clusters. The average expression of each gene was represented by color (low to high was shown as blue to red).

Computational analysis of human GBM datasets—For analysis of human GBM data, we downloaded the gene expression and survival data of TCGA datasets (Agilent-4502A or HG-U133A microarrays) or other available datasets from GlioVis: http://gliovis.bioinfo.cnio.es/. The expression, correlation, and survival analyses, and GSEA of interesting genes in GBM patients were performed using GlioVis. The TCGA GBM samples were clustered by using the 20-gene angiogenesis signature into angiogenesis-high and angiogenesis-low subgroups, using complete-linkage hierarchical clustering.

QUANTIFICATION AND STATISTICAL ANALYSIS

Statistical analyses were performed with Student's t-test for comparisons between two groups, and one-way ANOVA test for comparisons among groups. Data was represented as mean ± SD or SEM. The survival and correlation analyses in brain cancer datasets (including TCGA datasets) and animal models were performed using the Log rank (Mantel-Cox) test and the Pearson test, respectively (GraphPad Prism 9). p values were designated as *, $p < 0.05$; **, $p < 0.01$, and ***, $p < 0.001$; n.s., non-significant ($p > 0.05$).

Supplementary Material

Refer to Web version on PubMed Central for supplementary material.

ACKNOWLEDGMENTS

The authors thank Drs. Frederick Lang and Jian Hu for providing GSCs; Dr. Katherine Fitzgerald for providing TBK1-flox mice; Dr. Ralf Adams for providing Cdh5(PAC)-CreERT2 mice; and Li Cai for the help with the clustering. P.C. was supported by NIH R00 CA240896 and R01 NS124594; DoD Career Development Award W81XWH-21-1-0380; NIH P50CA221747; Cancer Research Foundation Young Investigator Award; Lynn Sage Scholar Award; American Cancer Society Institutional Research Grant IRG-21-144-27; philanthropic donations from Mindy Jacobson and the Bill Bass Foundation, Northwestern University start-up funds; and the Northwestern Medicine Malnati Brain Tumor Insitute of the Lurie Comprehensive Cancer Center. R.S.H. was supported by NIH 1K08HL143271 and R03HL155249.

REFERENCES

1. Chen P, Hsu WH, Chang A, Tan Z, Lan Z, Zhou A, Spring DJ, Lang FF, Wang YA, and DePinho RA (2020). Circadian regulator CLOCK recruits immune-suppressive microglia into the GBM tumor microenvironment. Cancer Discov. 10, 371–381. 10.1158/2159-8290.CD-19-0400. [PubMed: 31919052]
2. Chen P, Zhao D, Li J, Liang X, Li J, Chang A, Henry VK, Lan Z, Spring DJ, Rao G, et al. (2019). Symbiotic macrophage-glioma cell interactions reveal synthetic lethality in PTEN-null glioma. Cancer Cell 35, 868–884.e6. 10.1016/j.ccell.2019.05.003. [PubMed: 31185211]
3. Fernandes C, Costa A, Osorio L, Lago RC, Linhares P, Carvalho B, and Caeiro C (2017). Current standards of care in glioblastoma therapy. In Glioblastoma S. De Vleeschouwer, ed.. 10.15586/codon.glioblastoma.2017.ch11.
4. Wen PY, Weller M, Lee EQ, Alexander BM, Barnholtz-Sloan JS, Barthel FP, Batchelor TT, Bindra RS, Chang SM, Chiocca EA, et al. (2020). Glioblastoma in adults: a Society for Neuro-Oncology (SNO) and European Society of Neuro-Oncology (EANO) consensus review on

current management and future directions. Neuro Oncol. 22, 1073–1113. 10.1093/neuonc/noaa106. [PubMed: 32328653]

5. Stupp R, Taillibert S, Kanner A, Read W, Steinberg D, Lhermitte B, Toms S, Idbaih A, Ahluwalia MS, Fink K, et al. (2017). Effect of tumor-treating fields plus maintenance temozolomide vs maintenance temozolomide alone on survival in patients with glioblastoma: a randomized clinical trial. JAMA 318, 2306–2316. 10.1001/jama.2017.18718. [PubMed: 29260225]
6. Xuan W, Lesniak MS, James CD, Heimberger AB, and Chen P (2021). Context-dependent glioblastoma-macrophage/microglia symbiosis and associated mechanisms. Trends Immunol. 42, 280–292. 10.1016/j.it.2021.02.004. [PubMed: 33663953]
7. Suvà ML, and Tirosh I (2020). The glioma stem cell model in the era of single-cell genomics. Cancer Cell 37, 630–636. 10.1016/j.ccell.2020.04.001. [PubMed: 32396858]
8. Chen P, Hsu WH, Han J, Xia Y, and DePinho RA (2021). Cancer stemness meets immunity: from mechanism to therapy. Cell Rep. 34, 108597. 10.1016/j.celrep.2020.108597. [PubMed: 33406434]
9. Zhou W, Ke SQ, Huang Z, Flavahan W, Fang X, Paul J, Wu L, Sloan AE, McLendon RE, Li X, et al. (2015). Periostin secreted by glioblastoma stem cells recruits M2 tumour-associated macrophages and promotes malignant growth. Nat. Cell Biol. 17, 170–182. 10.1038/ncb3090. [PubMed: 25580734]
10. Khan F, Pang L, Dunterman M, Lesniak MS, Heimberger AB, and Chen P (2023). Macrophages and microglia in glioblastoma: heterogeneity, plasticity, and therapy. J. Clin. Invest. 133, e163446. 10.1172/JCI163446. [PubMed: 36594466]
11. Xuan W, Khan F, James CD, Heimberger AB, Lesniak MS, and Chen P (2021). Circadian regulation of cancer cell and tumor microenvironment crosstalk. Trends Cell Biol. 31, 940–950. 10.1016/j.tcb.2021.06.008. [PubMed: 34272133]
12. Xuan W, Hsu WH, Khan F, Dunterman M, Pang L, Wainwright DA, Ahmed AU, Heimberger AB, Lesniak MS, and Chen P (2022). Circadian regulator CLOCK drives immunosuppression in glioblastoma. Cancer Immunol. Res. 10, 770–784. 10.1158/2326-6066.CIR-21-0559. [PubMed: 35413115]
13. Dunn GP, Rinne ML, Wykosky J, Genovese G, Quayle SN, Dunn IF, Agarwalla PK, Chheda MG, Campos B, Wang A, et al. (2012). Emerging insights into the molecular and cellular basis of glioblastoma. Genes Dev. 26, 756–784. 10.1101/gad.187922.112. [PubMed: 22508724]
14. Cao Y, Arbiser J, D'Amato RJ, D'Amore PA, Ingber DE, Kerbel R, Klagsbrun M, Lim S, Moses MA, Zetter B, et al. (2011). Forty-year journey of angiogenesis translational research. Sci. Transl. Med. 3, 114rv3. 10.1126/scitranslmed.3003149.
15. Hambardzumyan D, and Bergers G (2015). Glioblastoma: defining tumor niches. Trends Cancer 1, 252–265. 10.1016/j.trecan.2015.10.009. [PubMed: 27088132]
16. Lucero R, Zappulli V, Sammarco A, Murillo OD, Cheah PS, Srinivasan S, Tai E, Ting DT, Wei Z, Roth ME, et al. (2020). Glioma-derived miRNA-containing extracellular vesicles induce angiogenesis by reprogramming brain endothelial cells. Cell Rep. 30, 2065–2074.e4. 10.1016/j.celrep.2020.01.073. [PubMed: 32075753]
17. Bao S, Wu Q, Sathornsumetee S, Hao Y, Li Z, Hjelmeland AB, Shi Q, McLendon RE, Bigner DD, and Rich JN (2006). Stem cell-like glioma cells promote tumor angiogenesis through vascular endothelial growth factor. Cancer Res. 66, 7843–7848. 10.1158/0008-5472.Can-06-1010. [PubMed: 16912155]
18. Cheng L, Huang Z, Zhou W, Wu Q, Donnola S, Liu JK, Fang X, Sloan AE, Mao Y, Lathia JD, et al. (2013). Glioblastoma stem cells generate vascular pericytes to support vessel function and tumor growth. Cell 153, 139–152. 10.1016/j.cell.2013.02.021. [PubMed: 23540695]
19. Wang Y, Sun N, Lu C, Bei Y, Qian R, and Hua L (2017). Upregulation of circadian gene 'hClock' contribution to metastasis of colorectal cancer. Int. J. Oncol. 50, 2191–2199. 10.3892/ijo.2017.3987. [PubMed: 28498393]
20. Jensen LD, Cao Z, Nakamura M, Yang Y, Bräutigam L, Andersson P, Zhang Y, Wahlberg E, Länne T, Hosaka K, and Cao Y (2012). Opposing effects of circadian clock genes bmal1 and period2 in regulation of VEGF-dependent angiogenesis in developing zebrafish. Cell Rep. 2, 231–241. 10.1016/j.celrep.2012.07.005. [PubMed: 22884368]

21. Dong Z, Zhang G, Qu M, Gimple RC, Wu Q, Qiu Z, Prager BC, Wang X, Kim LJY, Morton AR, et al. (2019). Targeting glioblastoma stem cells through disruption of the circadian clock. Cancer Discov. 9, 1556–1573. 10.1158/2159-8290.CD-19-0215. [PubMed: 31455674]

22. Liberzon A, Birger C, Thorvaldsdó ttir H, Ghandi M, Mesirov JP, and Tamayo P. (2015). The Molecular Signatures Database (MSigDB) hallmark gene set collection. Cell Syst. 1, 417–425. 10.1016/j.cels.2015.12.004. [PubMed: 26771021]

23. Cancer Genome Atlas Research Network (2008). Comprehensive genomic characterization defines human glioblastoma genes and core pathways. Nature 455, 1061–1068. 10.1038/nature07385. [PubMed: 18772890]

24. Shingu T, Ho AL, Yuan L, Zhou X, Dai C, Zheng S, Wang Q, Zhong Y, Chang Q, Horner JW, et al. (2017). Qki deficiency maintains stemness of glioma stem cells in suboptimal environment by downregulating endolysosomal degradation. Nat. Genet. 49, 75–86. 10.1038/ng.3711. [PubMed: 27841882]

25. Shi Q, Rafii S, Wu MH, Wijelath ES, Yu C, Ishida A, Fujita Y, Kothari S, Mohle R, Sauvage LR, et al. (1998). Evidence for circulating bone marrow-derived endothelial cells. Blood 92, 362–367. [PubMed: 9657732]

26. Seyfried TN, el-Abbadi M, Ecsedy JA, Bai HW, and Yohe HC (1996). Influence of host cell infiltration on the glycolipid content of mouse brain tumors. J. Neurochem. 66, 2026–2033. 10.1046/j.1471-4159.1996.66052026.x. [PubMed: 8780032]

27. Masiero M, Simões FC, Han HD, Snell C, Peterkin T, Bridges E, Mangala LS, Wu SYY, Pradeep S, Li D, et al. (2013). A core human primary tumor angiogenesis signature identifies the endothelial orphan receptor ELTD1 as a key regulator of angiogenesis. Cancer Cell 24, 229–241. 10.1016/j.ccr.2013.06.004. [PubMed: 23871637]

28. Neftel C, Laffy J, Filbin MG, Hara T, Shore ME, Rahme GJ, Richman AR, Silverbush D, Shaw ML, Hebert CM, et al. (2019). An integrative model of cellular states, plasticity, and genetics for glioblastoma. Cell 178, 835–849.e21. 10.1016/j.cell.2019.06.024. [PubMed: 31327527]

29. Abdelfattah N, Kumar P, Wang C, Leu JS, Flynn WF, Gao R, Baskin DS, Pichumani K, Ijare OB, Wood SL, et al. (2022). Single-cell analysis of human glioma and immune cells identifies S100A4 as an immunotherapy target. Nat. Commun. 13, 767, ARTN 767. 10.1038/s41467-022-28372-y. [PubMed: 35140215]

30. Clark K, Plater L, Peggie M, and Cohen P (2009). Use of the pharmacological inhibitor BX795 to study the regulation and physiological roles of TBK1 and IkappaB kinase epsilon: a distinct upstream kinase mediates Ser-172 phosphorylation and activation. J. Biol. Chem. 284, 14136–14146. 10.1074/jbc.M109.000414. [PubMed: 19307177]

31. Hasan M, and Yan N (2016). Therapeutic potential of targeting TBK1 in autoimmune diseases and interferonopathies. Pharmacol. Res. 111, 336–342. 10.1016/j.phrs.2016.04.008. [PubMed: 27353409]

32. Jenkins RW, Aref AR, Lizotte PH, Ivanova E, Stinson S, Zhou CW, Bowden M, Deng J, Liu H, Miao D, et al. (2018). Ex vivo profiling of PD-1 blockade using organotypic tumor spheroids. Cancer Discov. 8, 196–215. 10.1158/2159-8290.Cd-17-0833. [PubMed: 29101162]

33. Wang Y, Nakayama M, Pitulescu ME, Schmidt TS, Bochenek ML, Sakakibara A, Adams S, Davy A, Deutsch U, Lu€thi U, et al. (2010). Ephrin-B2 controls VEGF-induced angiogenesis and lymphangiogenesis. Nature 465, 483–486. 10.1038/nature09002. [PubMed: 20445537]

34. Schernhammer ES, Laden F, Speizer FE, Willett WC, Hunter DJ, Kawachi I, Fuchs CS, and Colditz GA (2003). Night-shift work and risk of colorectal cancer in the nurses' health study. J. Natl. Cancer Inst. 95, 825–828. [PubMed: 12783938]

35. Fu L, and Kettner NM (2013). The circadian clock in cancer development and therapy. Prog. Mol. Biol. Transl. Sci. 119, 221–282. 10.1016/B978-0-12-396971-2.00009-9. [PubMed: 23899600]

36. Puram RV, Kowalczyk MS, de Boer CG, Schneider RK, Miller PG, McConkey M, Tothova Z, Tejero H, Heckl D, Järås M, et al. (2016). Core circadian clock genes regulate leukemia stem cells in AML. Cell 165, 303–316. 10.1016/j.cell.2016.03.015. [PubMed: 27058663]

37. Li A, Lin X, Tan X, Yin B, Han W, Zhao J, Yuan J, Qiang B, and Peng X (2013). Circadian gene Clock contributes to cell proliferation and migration of glioma and is directly regulated by tumor-

suppressive miR-124. FEBS Lett. 587, 2455–2460. 10.1016/j.febslet.2013.06.018. [PubMed: 23792158]

38. Cao Y (2014). VEGF-targeted cancer therapeutics-paradoxical effects in endocrine organs. Nat. Rev. Endocrinol. 10, 530–539. 10.1038/nrendo.2014.114. [PubMed: 25048037]
39. Cao Y (2010). Off-tumor target–beneficial site for antiangiogenic cancer therapy? Nat. Rev. Clin. Oncol. 7, 604–608. 10.1038/nrclinonc.2010.118. [PubMed: 20683436]
40. Cao Y (2009). Tumor angiogenesis and molecular targets for therapy. Front. Biosci. 14, 3962–3973. 10.2741/3504.
41. Kaka N, Hafazalla K, Samawi H, Simpkin A, Perry J, Sahgal A, and Das S (2019). Progression-free but No overall survival benefit for adult patients with bevacizumab therapy for the treatment of newly diagnosed glioblastoma: a systematic review and meta-analysis. Cancers 11, 1723, ARTN 1723. 10.3390/cancers11111723. [PubMed: 31689995]
42. Zerrouqi A, Pyrzynska B, Febbraio M, Brat DJ, and Van Meir EG (2012). P14ARF inhibits human glioblastoma-induced angiogenesis by upregulating the expression of TIMP3. J. Clin. Invest. 122, 1283–1295. 10.1172/JCI38596. [PubMed: 22378045]
43. Bonavia R, Inda MM, Vandenberg S, Cheng SY, Nagane M, Hadwiger P, Tan P, Sah DWY, Cavenee WK, and Furnari FB (2012). EGFRvIII promotes glioma angiogenesis and growth through the NF-kappaB, interleukin-8 pathway. Oncogene 31, 4054–4066. 10.1038/onc.2011.563. [PubMed: 22139077]
44. Liu Y, Li F, Gao F, Xing L, Qin P, Liang X, Zhang J, Qiao X, Lin L, Zhao Q, and Du L (2016). Periostin promotes tumor angiogenesis in pancreatic cancer via Erk/VEGF signaling. Oncotarget 7, 40148–40159. 10.18632/oncotarget.9512. [PubMed: 27223086]
45. Keklikoglou I, Kadioglu E, Bissinger S, Langlois B, Bellotti A, Orend G, Ries CH, and De Palma M (2018). Periostin limits tumor response to VEGFA inhibition. Cell Rep. 22, 2530–2540. 10.1016/j.celrep.2018.02.035. [PubMed: 29514082]
46. Park SY, Piao Y, Jeong KJ, Dong J, and de Groot JF (2016). Periostin (POSTN) regulates tumor resistance to antiangiogenic therapy in glioma models. Mol. Cancer Ther. 15, 2187–2197. 10.1158/1535-7163.Mct-15-0427. [PubMed: 27307601]
47. Liu AY, Zheng H, and Ouyang G (2014). Periostin, a multifunctional matricellular protein in inflammatory and tumor microenvironments. Matrix Biol. 37, 150–156. 10.1016/j.matbio.2014.04.007. [PubMed: 24813586]
48. Gillan L, Matei D, Fishman DA, Gerbin CS, Karlan BY, and Chang DD (2002). Periostin secreted by epithelial ovarian carcinoma is a ligand for alpha(V)beta(3) and alpha(V)beta(5) integrins and promotes cell motility. Cancer Res. 62, 5358–5364. [PubMed: 12235007]
49. Hagan RS, Torres-Castillo J, and Doerschuk CM (2019). Myeloid TBK1 signaling contributes to the immune response to influenza. Am. J. Respir. Cell Mol. Biol. 60, 335–345. 10.1165/rcmb.2018-0122OC. [PubMed: 30290124]
50. Hiscott J (2007). Triggering the innate antiviral response through IRF-3 activation. J. Biol. Chem. 282, 15325–15329. 10.1074/jbc.R700002200. [PubMed: 17395583]
51. Li X, Zhang Q, Ding Y, Liu Y, Zhao D, Zhao K, Shen Q, Liu X, Zhu X, Li N, et al. (2016). Methyltransferase Dnmt3a upregulates HDAC9 to deacetylate the kinase TBK1 for activation of antiviral innate immunity. Nat. Immunol. 17, 806–815. 10.1038/ni.3464. [PubMed: 27240213]
52. Eskiocak B, McMillan EA, Mendiratta S, Kollipara RK, Zhang H, Humphries CG, Wang C, Garcia-Rodriguez J, Ding M, Zaman A, et al. (2017). Biomarker accessible and chemically addressable mechanistic subtypes of BRAF melanoma. Cancer Discov. 7, 832–851. 10.1158/2159-8290.Cd-16-0955. [PubMed: 28455392]
53. Cooper JM, Ou YH, McMillan EA, Vaden RM, Zaman A, Bodemann BO, Makkar G, Posner BA, and White MA (2017). TBK1 provides context-selective support of the activated AKT/mTOR pathway in lung cancer. Cancer Res. 77, 5077–5094. 10.1158/0008-5472.Can-17-0829. [PubMed: 28716898]
54. Cruz VH, and Brekken RA (2018). Assessment of TANK-binding kinase 1 as a therapeutic target in cancer. J. Cell Commun. Signal. 12, 83–90. 10.1007/s12079-017-0438-y. [PubMed: 29218456]
55. Alvarado AG, Thiagarajan PS, Mulkearns-Hubert EE, Silver DJ, Hale JS, Alban TJ, Turaga SM, Jarrar A, Reizes O, Longworth MS, et al. (2017). Glioblastoma cancer stem cells evade innate

immune suppression of self-renewal through reduced TLR4 expression. Cell Stem Cell 20, 450–461.e4. 10.1016/j.stem.2016.12.001. [PubMed: 28089910]

56. Korherr C, Gille H, Schäfer R, Koenig-Hoffmann K, Dixelius J, Egland KA, Pastan I, and Brinkmann U (2006). Identification of proangiogenic genes and pathways by high-throughput functional genomics: TBK1 and the IRF3 pathway. Proc. Natl. Acad. Sci. USA 103, 4240–4245. 10.1073/pnas.0511319103. [PubMed: 16537515]
57. Czabanka M, Korherr C, Brinkmann U, and Vajkoczy P (2008). Influence of TBK-1 on tumor angiogenesis and microvascular inflammation. Front. Biosci. 13, 7243–7249. 10.2741/3225. [PubMed: 18508731]
58. Ancuta P, Rao R, Moses A, Mehle A, Shaw SK, Luscinskas FW, and Gabuzda D (2003). Fractalkine preferentially mediates arrest and migration of CD16+ monocytes. J. Exp. Med. 197, 1701–1707. 10.1084/jem.20022156. [PubMed: 12810688]
59. Yang L, Froio RM, Sciuto TE, Dvorak AM, Alon R, and Luscinskas FW (2005). ICAM-1 regulates neutrophil adhesion and transcellular migration of TNF-alpha-activated vascular endothelium under flow. Blood 106, 584–592. 10.1182/blood-2004-12-4942. [PubMed: 15811956]
60. Chen P, Huang Y, Bong R, Ding Y, Song N, Wang X, Song X, and Luo Y (2011). Tumor-associated macrophages promote angiogenesis and melanoma growth via adrenomedullin in a paracrine and autocrine manner. Clin. Cancer Res. 17, 7230–7239. 10.1158/1078-0432.CCR-11-1354. [PubMed: 21994414]
61. Varghese F, Bukhari AB, Malhotra R, and De A (2014). IHC profiler: an open source plugin for the quantitative evaluation and automated scoring of immunohistochemistry images of human tissue samples. PLoS One 9, e96801. 10.1371/journal.pone.0096801. [PubMed: 24802416]
62. Barth ND, Subiros-Funosas R, Mendive-Tapia L, Duffin R, Shields MA, Cartwright JA, Henriques ST, Sot J, Goñi FM, Lavilla R, et al. (2020). A fluorogenic cyclic peptide for imaging and quantification of drug-induced apoptosis. Nat. Commun. 11, 4027. 10.1038/s41467-020-17772-7. [PubMed: 32788676]

Highlights

- The CLOCK-BMAL1 complex promotes tumor angiogenesis in GBM
- CLOCK-directed OLFML3-HIF1α axis upregulates pro-angiogenic factor POSTN
- POSTN promotes angiogenesis via activation of the TBK1 signaling in endothelial cells
- Inhibition of the CLOCK-directed POSTN-TBK1 axis impairs GBM progression and angiogenesis

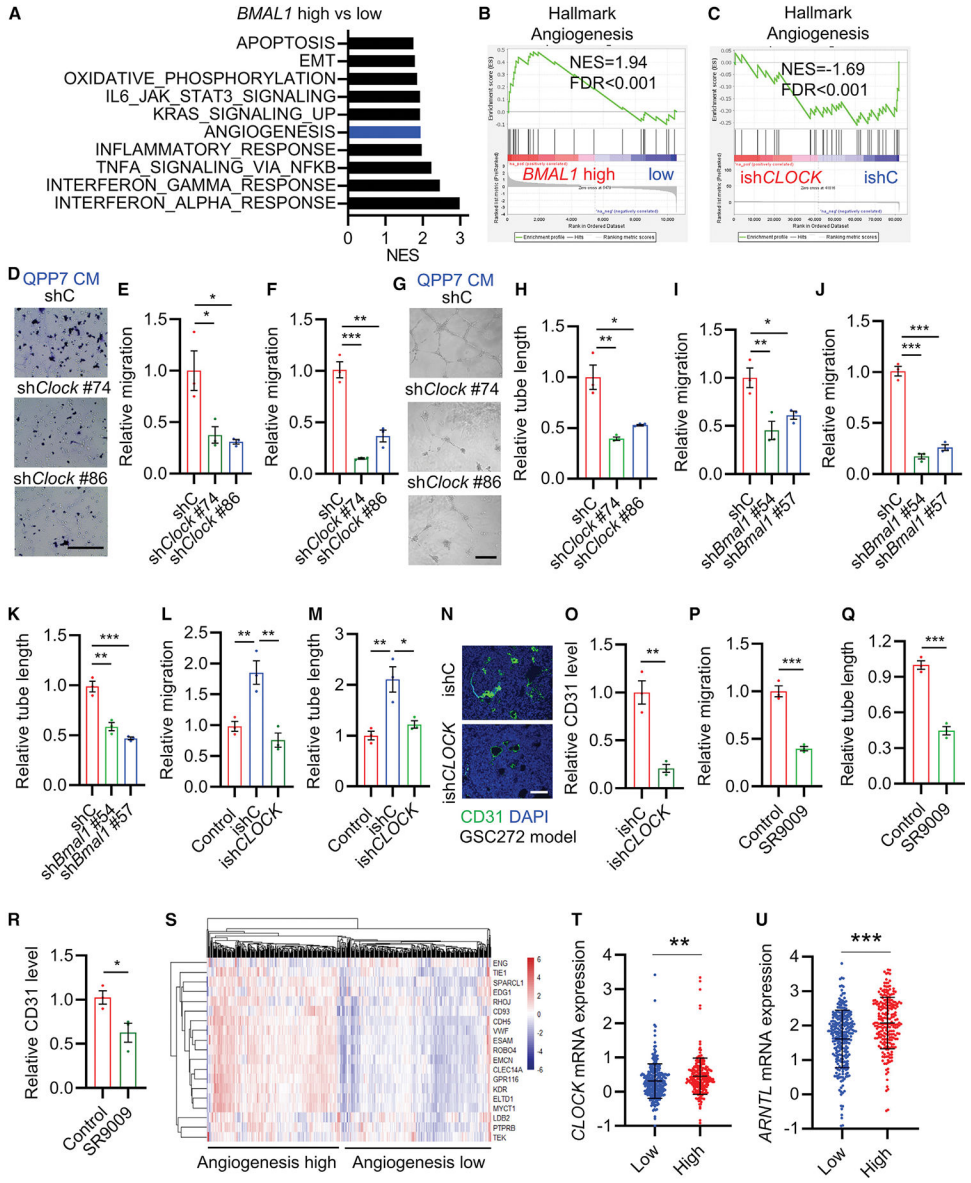

Figure 1. GSC-derived CLOCK promotes angiogenesis in GBM

(A) GSEA analysis on TCGA GBM patient tumors shows the top 10 enriched hallmark pathways in *BMAL1*-high (the upper quartile) patients compared with *BMAL1*-low (the lower quartile) patients. Blue highlighted pathway relates to angiogenesis.

(B) GSEA shows enrichment of angiogenesis signature in *BMAL1*-high patient tumors compared with *BMAL1*-low patient tumors. The normalized enrichment score (NES) and false discovery rate (FDR) q value of correlation are shown.

(C) GSEA shows enrichment of angiogenesis signature in GSC272 cells harboring an inducible *CLOCK* shRNA (ish*CLOCK*) compared with ish control (ishC). NES and FDR q value of correlation are shown.

(D and E) Representative images (D) and quantification (E) of relative migration of primary mouse brain endothelial cells following stimulation with conditioned media (CMs) from

QPP7 GSCs expressing control shRNA (shC) and *Clock* shRNAs (sh*Clock*). Scale bar, 200 μm; n = 3 biological replicates.

(F) Quantification of relative migration of iHUVECs following stimulation with CMs from QPP7 GSCs expressing shC and sh*Clock*. n = 3 biological replicates.

(G and H) Representative images (G) and quantification (H) of relative tube formation of iHUVECs following stimulation with CMs from QPP7 GSCs expressing control shC and sh*Clock*. Scale bar, 200 μm; n = 3 biological replicates.

(I) Quantification of relative migration of primary mouse brain endothelial cells following stimulation with CMs from QPP7 GSCs expressing shC and sh*Bmal1*. n = 3 biological replicates.

(J) Quantification of relative migration of iHUVECs following stimulation with CMs from QPP7 GSCs expressing shC and sh*Bmal1*. n = 3 biological replicates.

(K) Quantification of relative tube formation of iHUVECs following stimulation with CMs from QPP7 GSCs expressing control shC and sh*Bmal1*. n = 3 biological replicates.

(L and M) Quantification of relative migration (L) and tube formation (M) of iHUVECs following stimulation with CMs from GSC272 cells expressing with or without ishC and ish*CLOCK*. n = 3 biological replicates.

(N and O) Immunofluorescence (N) and quantification (O) of CD31 in tumors from SCID mice implanted with ish*CLOCK* and ishC GSC272 models. Scale bar, 100 μm; n = 3 biological replicates.

(P) Quantification of relative migration of iHUVECs following stimulation with CMs from GSC272 cells treated with or without SR9009 (5 μM). n = 3 biological replicates.

(Q) Quantification of relative tube formation of iHUVECs following stimulation with CMs from GSC272 cells treated with or without SR9009 (5 μM). n = 3 biological replicates.

(R) Quantification of CD31 in tumors from CT2A-bearing C57BL/6J mice treated with or without SR9009 (100 mg/kg, intraperitoneally [i.p.], daily) for 10 days beginning at day 7 post-orthotopic injection. n = 3 biological replicates.

(S) Clustering of human TCGA GBM tumor samples into angiogenesis-high and angiogenesis-low groups with use of a 20-gene angiogenesis signature.

(T) The expression of *CLOCK* in angiogenesis-high versus angiogenesis-low patient tumors.

(U) The expression of *ARNTL* in angiogenesis-high versus angiogenesis-low patient tumors.

Data from multiple replicates are presented as mean. Error bars indicate mean ± SEM or SD. *p < 0.05, **p < 0.01, ***p < 0.001, Student’s t test and/or one-way ANOVA test.

See also Figures S1 and S2.

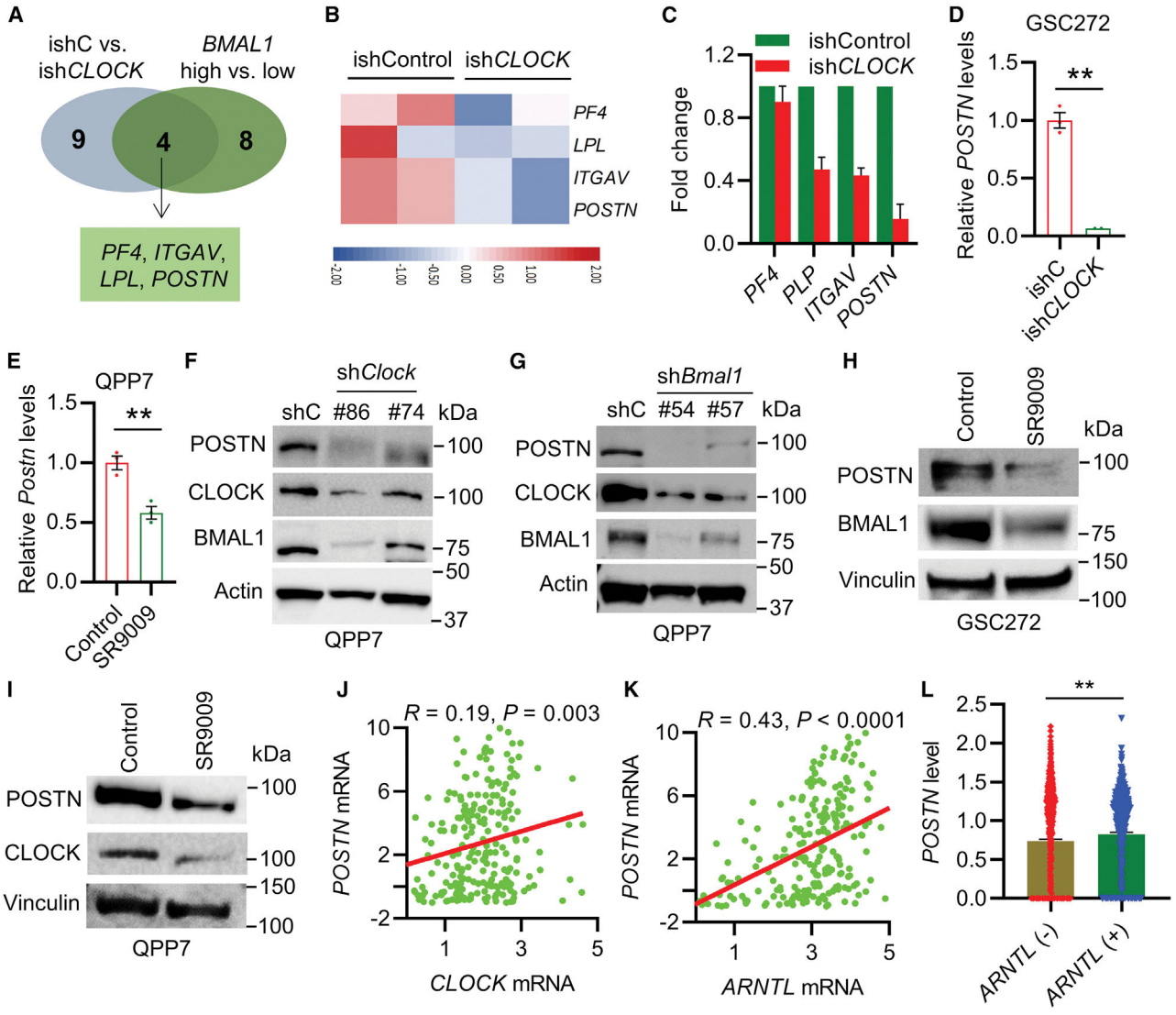

Figure 2. The CLOCK-BMAL1 complex upregulates pro-angiogenetic factor POSTN in GSCs

(A) Identification of four overlapping angiogenic factors in ish*CLOCK* versus ishC GSC272 cells and in *BMAL1*-high versus *BMAL1*-low TCGA GBM patient tumors.

(B) Heatmap representation of the four angiogenesis signature genes in ish*CLOCK* GSC272 cells compared with ishC cells. Red signal indicates higher expression, and blue signal denotes lower expression.

(C) mRNA levels of the four angiogenesis signature genes in ish*CLOCK* and ishC GSC272 cells. n = 2 biological replicates. *POSTN* shows the most dramatic reduction upon CLOCK depletion.

(D) qRT-PCR shows the expression of *POSTN* in ishC and ish*CLOCK* GSC272 cells. n = 3 biological replicates. Values are expressed as relative expression levels with respect to housekeeping gene *ACTB*.

(E) qRT-PCR shows the expression of *Postn* in control- and SR9009 (5 μM)-treated QPP7 GSCs. n = 3 biological replicates. Values are expressed as relative expression levels with respect to housekeeping gene *Actb*.

(F) Immunoblots for CLOCK, BMAL1, and POSTN in lysates of QPP7 GSCs expressing shC and sh*Clock*.

(G) Immunoblots for CLOCK, BMAL1, and POSTN in lysates of QPP7 GSCs expressing shC and sh*Bmal1*.

(H and I) Immunoblots for CLOCK, BMAL1, and POSTN in lysates of GSC272 cells (H) and QPP7 GSCs (I) treated with or without SR9009 (5 μM).

(J) The correlation of *CLOCK* and *POSTN* in CGGA GBM patient tumors. *R* and p values are shown. Pearson test.

(K) The correlation of *ARNTL* and *POSTN* in CGGA GBM patient tumors. *R* and p values are shown. Pearson test.

(L) *POSTN* expression in *ARNTL* (−) and *ARNTL* (+) GSCs. The analysis is based on single-cell RNA sequencing data from 28 patients with GBM. **p < 0.01, Student's t test.

Data from multiple replicates are presented as mean. Error bars indicate mean ± SEM. *p < 0.05, **p < 0.01, Student's t test.

See also Figure S3.

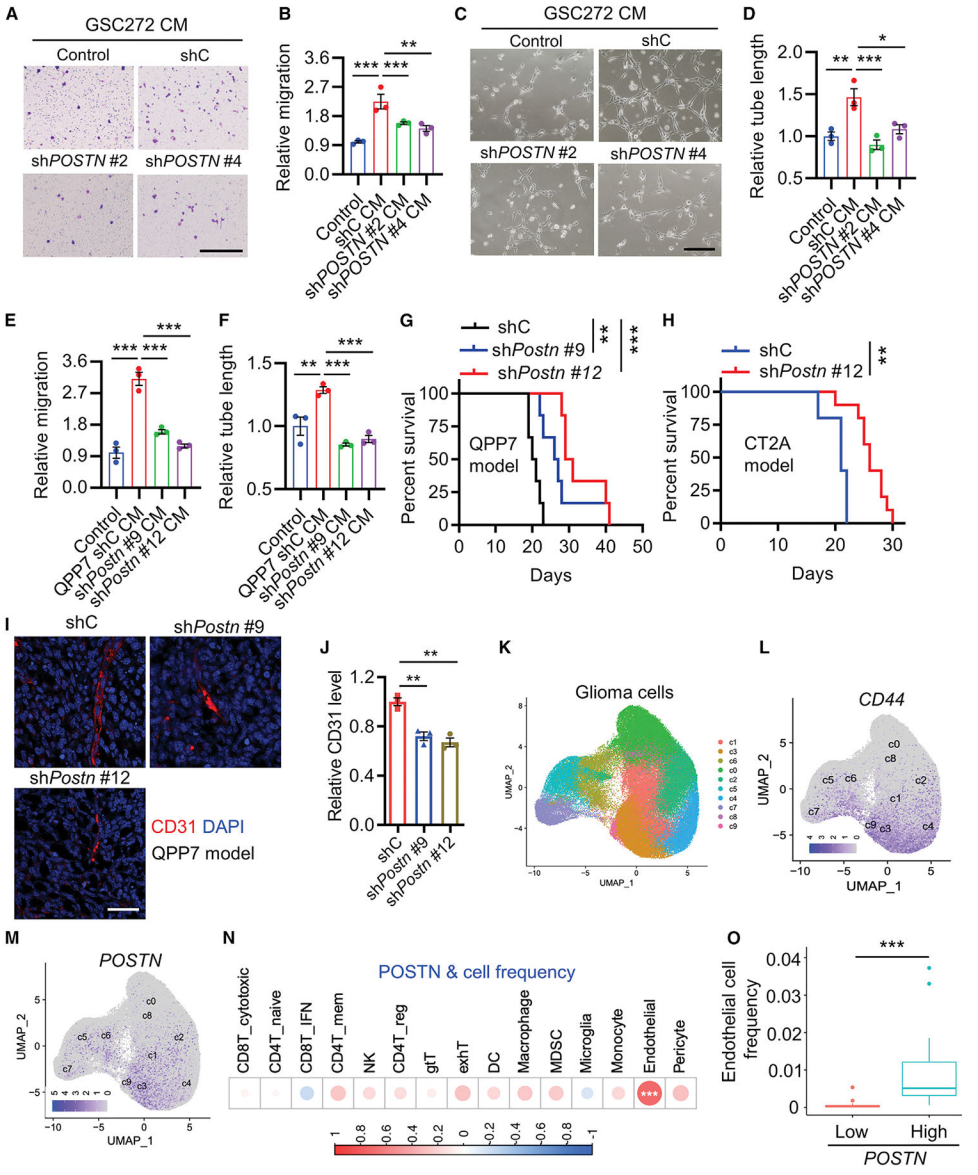

Figure 3. POSTN in GSCs is essential for angiogenesis and tumor progression

(A and B) Representative images (A) and quantification (B) of relative migration of iHUVECs following stimulation with CMs from GSC272 cells expressing shC and sh*POSTN*. Scale bar, 200 μm; n = 3 biological replicates.

(C and D) Representative images (C) and quantification (D) of relative tube formation of iHUVECs following stimulation with CMs from GSC272 cells expressing shC and sh*POSTN*. Scale bar, 400 μm; n = 3 biological replicates.

(E and F) Quantification of relative Transwell migration (E) and tube formation (F) of iHUVECs following stimulation with CMs from QPP7 GSCs expressing shC and sh*Postn*. n = 3 biological replicates.

(G) Survival curves of C57BL/6 mice implanted with QPP7 GSCs (2×10^4 cells) expressing shC and sh*Postn* (n = 6–7 mice per group).

(H) Survival curves of C57BL/6 mice implanted with CT2A cells (2×10^4 cells) expressing shC and sh*Postn* (n = 5 mice for shC group and 10 mice for sh*Postn* group).
(I and J) Immunofluorescence (I) and quantification (J) of CD31 in tumors from C57BL/6J implanted with shC and sh*Postn* QPP7 GSCs. Scale bar, 50 μm; n = 3 biological replicates.
(K–M) High-resolution uniform manifold approximation and projection (UMAP) dimensional reduction of glioma cells from GBM patient tumors, partitioned into nine distinct clusters (K). The expression of *CD44* (L) and *POSTN* (M) in glioma cells/GSCs are shown. Intensity of the blue color indicates the expression of individual cells. The analysis was performed on single-cell RNA sequencing data of glioma cells from samples of 16 patients with GBM.
(N) The correlation between glioma cell/GSC *POSTN* level and the frequency of tumor microenvironment components (including immune cells, endothelial cells, and pericytes as indicated) based on single-cell RNA sequencing data from 16 GBM patient tumors. Red signal indicates positive correlation, and blue signal denotes negative correlation.
(O) Endothelial cell frequency in patients with glioma with glioma cell/GSC *POSTN* high versus *POSTN* low. The analysis is based on single-cell RNA sequencing data from 16 GBM patient tumors.
Data from multiple replicates are presented as mean. Error bars indicate mean ± SEM. *p < 0.05, **p < 0.01, ***p < 0.001, one-way ANOVA test (B and D–F), Student's t test (O), and log rank test (G and H).
See also Figures S4–S6.

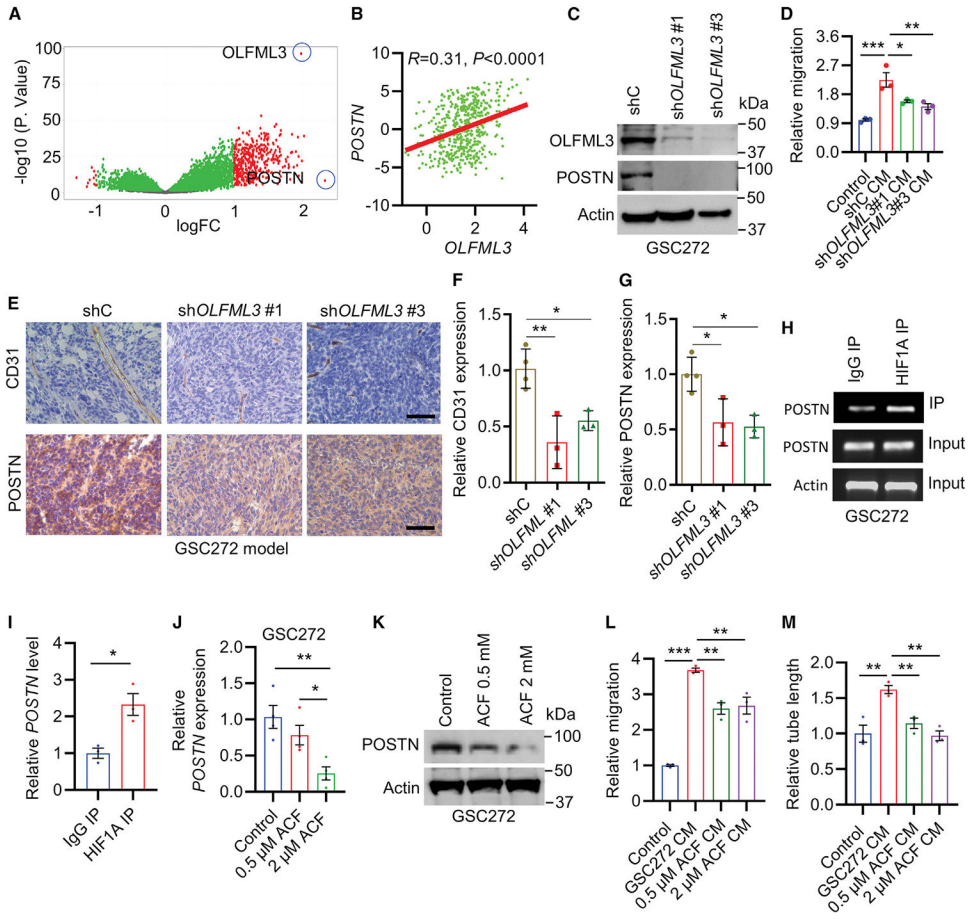

Figure 4. CLOCK-directed OLFML3-HIF1α axis upregulates POSTN expression and angiogenesis

(A) Volcano plots showing the fold change of genes (log2 scale) between *OLFML3*-high and *OLFML3*-low patient tumors (y axis, log10 scale). *POSTN* is the top one highly expressed in *OLFML3*-high tumors.

(B) The correlation of *POSTN* and *OLFML3* in TCGA GBM patient tumors. *R* and p values are shown. Pearson test.

(C) Immunoblots for OLFML3 and POSTN in lysates of GSC272 cells expressing shC and sh*OLFML3*.

(D) Quantification of relative Transwell migration of iHUVECs following stimulation with CMs from GSC272 cells expressing shC and sh*OLFML3*. n = 3 biological replicates.

(E) Immunohistochemistry staining for CD31 (top panels) and POSTN (bottom panels) in tumors from SCID mice implanted with sh*OLFML3* and shC GSC272 cells. Scale bar, 100 μm.

(F and G) Quantification of immunohistochemistry staining for CD31 (F) and POSTN (G) in tumors from SCID mice implanted with sh*OLFML3* and shC GSC272 cells. n = 3 biological replicates.

(H and I) Representative images (H) and quantification (I) of HIF1A ChIP-PCR in the *POSTN* promoter of GSC272 cells. n = 3 biological replicates.

(J) qRT-PCR for *POSTN* in lysates of GSC272 cells treated with HIF1α inhibitor acriflavine (ACF) at indicated concentrations. n = 3 biological replicates. Values are expressed as relative expression levels with respect to housekeeping gene *ACTB*.

(K) Immunoblots for POSTN in lysates of GSC272 cells treated with ACF at indicated concentrations.

(L and M) Quantification of relative Transwell migration (L) and tube formation (M) of iHUVECs following stimulation with CMs from GSC272 cells treated with or without ACF at indicated concentrations. n = 3 biological replicates.

Data from multiple replicates are presented as mean. Error bars indicate mean ± SEM. *p < 0.05, **p < 0.01, ***p < 0.001, one-way ANOVA test (D, F, G, J, L, and M) and Student's t test (I).

See also Figure S7.

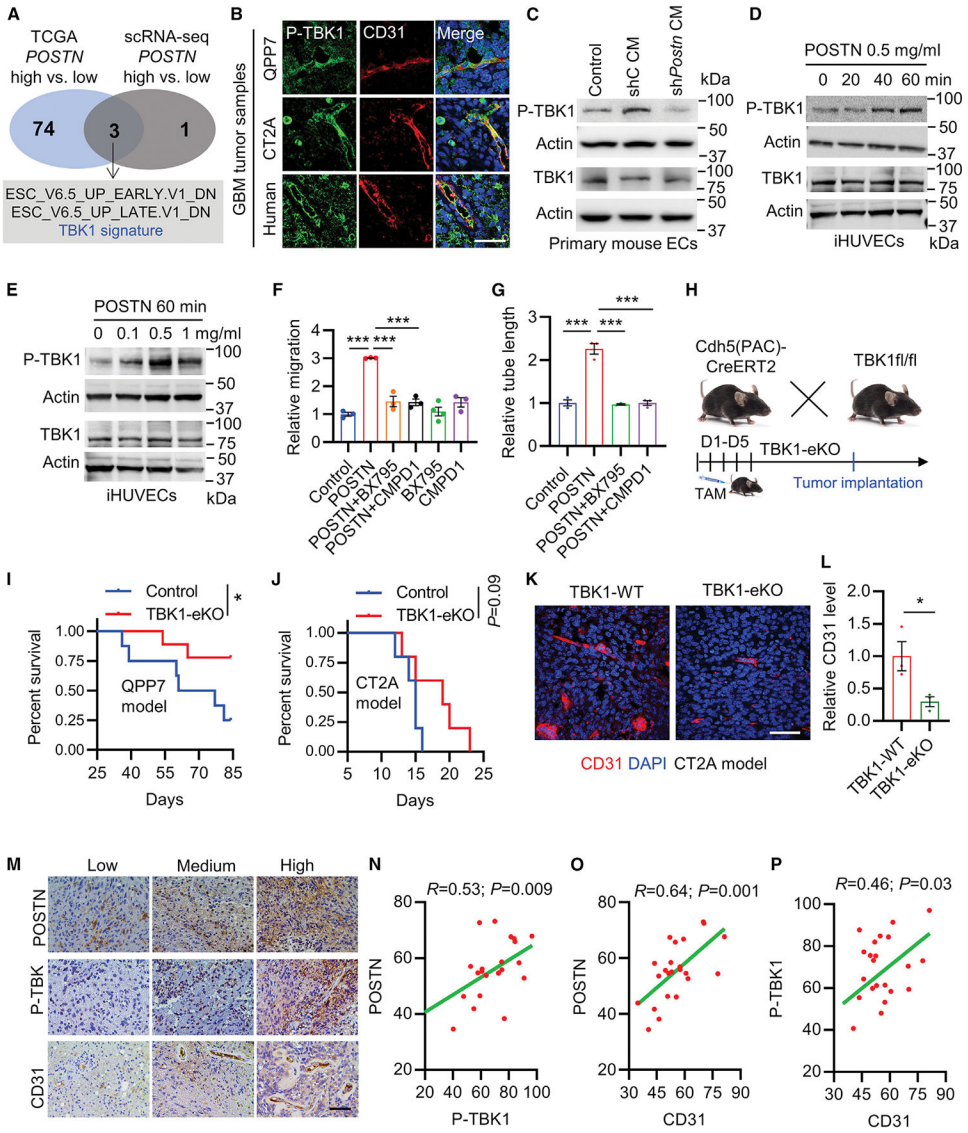

Figure 5. TBK1 mediates POSTN-induced angiogenesis in GBM

(A) Identification of the overlapping signature pathways in TCGA GBM patient tumors (*POSTN* high versus *POSTN* low) and in endothelial cells from single-cell RNA sequencing (scRNA-seq) data of GBM patient tumors (glioma cell/GSC *POSTN* high versus *POSTN* low).

(B) Co-immunofluorescence for P-TBK1 and CD31 in QPP7 and CT2A tumors established in C57BL/6J mice (top and middle panels) and in GBM patient tumors (bottom panels). Scale bar, 50 μm.

(C) Immunoblots for TBK1 and P-TBK1 in lysates of primary mouse brain endothelial cells treated with or without CMs from CT2A cells expressing shC and sh*Postn*.

(D and E) Immunoblots for TBK1 and P-TBK1 in lysates of iHUVECs treated with POSTN recombinant protein at 500 ng/mL for different time points (D) and for 60 min at different concentrations (E).

(F and G) Quantification of relative Transwell migration (F) and tube formation (G) of iHUVECs following stimulation with POSTN recombinant protein (500 ng/mL) in the presence or absence of TBK1 inhibitor BX795 (1 μM) and CMPD1 (1 μM). n = 3 biological replicates.

(H) Schematic of generation of endothelial cell-specific TBK1 knockout (TBK1-eKO) mice by crossing TBK1fl/fl mice with Cdh5(PAC)-CreERT2 mice. TBK1 KO in endothelial cells is induced by injection of tamoxifen (TAM; 75 mg/kg i.p.) for 5 days.

(I and J) Survival curves of TBK1-WT and TBK1-eKO mice implanted with 2×10^4 QPP7 GSCs (I, n = 8–9 mice/group) and CT2A cells (J, n = 5 mice/group).

(K and L) Immunofluorescence (K) and quantification (L) of relative CD31 in tumors from TBK1-WT and TBK1-eKO mice implanted with CT2A cells. Scale bar, 50 μm n = 3 biological replicates.

(M) Representative images show low, medium, and high expression of POSTN, P-TBK1, and CD31 in human GBM tumor samples based on immunohistochemistry staining. Scale bar, 100 μm.

(N–P) Quantification of immunohistochemistry staining showing strong positive correlation between POSTN and P-TBK1 (N), POSTN and CD31 (O), and P-TBK1 and CD31 (P) in human GBM tumor samples (n = 23). *R* and p values are shown. Pearson test.

Data from multiple replicates are presented as mean. Error bars indicate mean ± SEM. *p < 0.05, **p < 0.01, ***p < 0.001, one-way ANOVA test (F and G), Student's t test (L), and log rank test (I and J).

See also Figure S8.

KEY RESOURCES TABLE

REAGENT or RESOURCE	SOURCE	IDENTIFIER
Antibodies		
POSTN	Novus Biologicals	Cat#NBP1-30042; RRID:AB_2166656
HIF1a	Cell Signaling	Cat#3716S; RRID:AB_2116962
TBK1	Cell Signaling	Cat#3013S; RRID:AB_2199749
P-TBK1	Cell Signaling	Cat#5483S; RRID:AB_10693472
OLFML3	Thermo Fisher Scientific	Cat# PA5-31581; RRID:AB_2549054
BMAL1	Cell Signaling	Cat#14020S; RRID:AB_2728705
CLOCK	Cell Signaling	Cat#5157S; RRID:AB_10695411
β-ACTIN	Cell Signaling	Cat# 3700S; RRID:AB_2242334
Vinculin	Cell Signaling	Cat#13901S; RRID:AB_2728768
CD31	Novus Biologicals	Cat#NBP2-80640; RRID:AB_2927581
Anti-mouse IgG, HRP-Linked	Cell Signaling	Cat#7076S; RRID:AB_330924
Anti-rabbit IgG, HRP-linked	Cell Signaling	Cat#7074S; RRID:AB_2099233
Anti-rabbit IgG, Alexa Fluor® 594 Conjugate	Cell Signaling	Cat#8889S; RRID:AB_2716249
Anti-rabbit IgG, Alexa Fluor ® 488 Conjugate	Cell Signaling	Cat#4412S; RRID:AB_1904025
Anti-mouse IgG, Alexa Fluor® 594 Conjugate	Cell Signaling	Cat#8890S; RRID:AB_2714182
Anti-rat IgG, Alexa Fluor ® 647	Thermo Fisher Scientific	Cat# A-21247 RRID:AB_141778
F4/80	Cell Signaling	Cat# 70076S RRID:AB_2799771
CD206	R&D Systems	Cat#AF2535 RRID:AB_2063012
Biological samples		
Human patient tumor samples (n = 23) from surgically resected IDH-WT GBMs. See Table S1.	Northwestern Central Nervous System Tissue Bank	N/A
Chemicals, peptides, and recombinant proteins		
Endothelial cell growth supplement	Corning	Cat#356006; CAS:N/A
Human fibroblast growth factor basic recombinant protein	R&D Systems	Cat#233-FB; CAS:N/A
Human Epidermal growth factor recombinant protein	R&D Systems	Cat#236-EG; CAS:N/A
Collagenase I	USP	Cat#1148089; CAS: N/A
Collagenase II	MP Biomedicals	Cat#0210050201; CAS: 2,593,923
Deoxyribonuclease I	Worthington	Cat#LS002139; CAS: 9003-98-9
CD45 MicroBeads	Miltenyi Biotec	Cat#130-052-301; CAS: N/A
CD31 MicroBeads	Miltenyi Biotec	Cat#130-097-418 CAS:N/A
Recombinant human POSTN protein	R&D Systems	Cat# 3548-F2-050 CAS:N/A
BX795	Selleck Chemicals	Cat# S1274 CAS: 702,675-74-9
TBK1/IKKε-IN-1 (Compound 1)	Selleck Chemicals	Cat# S8922 CAS: 1,893,397-65-3
SR9009	Selleck Chemicals	Cat# S8692
Acriflavine (ACF)	Sigma -Aldrich	Cat# A8126 CAS: 8048-52-0

REAGENT or RESOURCE	SOURCE	IDENTIFIER
Propidium iodide (PI)	BioLegend	Cat# 421301 CAS:N/A
Critical commercial assays		
BCA protein assay kit	Thermo Fisher Scientific	Cat#23225
Pierce ™ Magnetic ChIP Kit	Thermo Fisher Scientific	Cat# 26157
Apotracker™ Green	BioLegend	Cat# 427402
CellTrace™ CFSE Cell Proliferation Kit	Invitrogen	Cat# C34554
EasySep™ Mouse Hematopoietic Progenitor Cell Isolation Kit	STEMCELL Technologies	Cat# 19856
Deposited data		
ChIP–seq data	Dong et al.[21]	GSE134974
Gene expression microarray data	Chen et al.[1]	GEO, GSE140409
Single-cell sequencing data	Neftel et al.[28]	GEO, GSE131928
Single-cell sequencing data	Abdelfattah et al.[29]	GEO, GSE182109
TCGA and CGGA expression and survival data	http://gliovis.bioinfo.cnio.es/	N/A
Experimental models: Cell lines		
293T	ATCC	Cat#CRL-11268; RRID:CVC_1926
QPP7	Laboratory of Dr. Jian Hu (MDACC)	N/A
GSC272	Laboratory of Dr. Frederick Lang (MDACC)	N/A
Immortalized human umbilical view endothelial cells (iHUVEC)	Laboratory of Dr. William A. Muller	N/A
CT2A	Seyfried et al.[26]	N/A
Human CD34+ Cells	STEMCELL Technologies	Cat# 70002.1
Experimental models: Organisms/strains		
Mouse C57BL/6	Jackson Laboratory	0,000,664
Mouse J:NU	Jackson Laboratory	007,850
Mouse ICR SCID	Taconic Biosciences	ICRSC-F
MouseC57BL/6 TBK1-flox	Laboratory of Dr. Katherine Fitzgerald (University of Massachusetts)	N/A
Mouse Cdh5(PAC)-CreERT2	Laboratory of Dr. William A. Muller (Northwestern University)	Developed by Dr. Ralf Adams (Max Planck Institute)
Oligonucleotides		
See Table S2	This paper	N/A
Recombinant DNA		
psPAX2	Addgene	Cat#12260
pMD2.G	Addgene	Cat#12259
pLKO.1 vector, Gateway Cloning System	Thermo Fisher Scientific	Cat#12535029
pLKO.1-puro	Sigma Aldrich	Cat#SHC001

REAGENT or RESOURCE	SOURCE	IDENTIFIER
pLKO.1-puro-human-*CLOCK* shRNA	Sigma-Aldrich	TRCN0000306475
pLKO.1-puro-human-*OLFML3* shRNA #1	Sigma-Aldrich	TRCN0000186745
pLKO.1-puro-human-*OLFML3* shRNA #3	Sigma-Aldrich	TRCN0000203502
pLKO.1-puro-human-*POSTN* shRNA #2	Sigma-Aldrich	TRCN0000123055
pLKO.1-puro-human-*POSTN* shRNA #4	Sigma-Aldrich	TRCN0000123057
pLKO.1-puro-mouse- *Clock* shRNA #74	Sigma-Aldrich	TRCN0000095686
pLKO.1-puro-mouse- *Clock* shRNA #86	Sigma-Aldrich	TRCN0000306474
pLKO.1-puro-mouse- *Bmal1* shRNA #54	Sigma-Aldrich	TRCN0000095054
pLKO.1-puro-mouse- *Bmal1* shRNA #57	Sigma-Aldrich	TRCN0000095057
pLKO.1-puro-mouse- *Postn* shRNA #9	Sigma-Aldrich	TRCN0000111166
pLKO.1-puro-mouse- *Postn* shRNA #12	Sigma-Aldrich	TRCN0000111169
Software and algorithms		
Prism GraphPad 9	Prism	https://www.graphpad.com/scientific-software/prism/
DESeq2 v 1.30.0	Bioconductor	https://bioconductor.org/packages/release/bioc/html/DESeq2.html
Image Lab	Bio-Rad	https://www.bio-rad.com/en-us/product/image-lab-software?ID=KRE6P5E8Z
Integrative Genomics Viewer (IGV)	Broad Institute	http://software.broadinstitute.org/software/igv/
Transcriptome Analysis Console	Affymetrix	https://www.thermofisher.com/us/en/home/life-science/microarray-analysis/microarray-analysis-instruments-software-services/microarray-analysis-software.html
Data Visualization Tools for Brain Tumor Datasets	http://gliovis.bioinfo.cnio.es/	N/A
GSEA-4.1.0	Broad Institute	http://software.broadinstitute.org/gsea/index.jsp
R package	The R Project for Statistical Computing	https://www.r-project.org/
ImageJ	NIH	https://imagej.net/Fiji